Doctoral Dissertation

博士論文

Neural circuit mechanisms of attractive social behavior in the main olfactory system

（主嗅覚系を介した社会行動を引き起こす神経回路の形成メカニズム）

Kasumi Inokuchi (Kato)

井ノ口 (加藤)　霞

Abstract

Odor information induces various innate responses that are critical to the survival of the individual and for the species. The medial amygdala (MeA) in rodents is known to mediate social behaviors by receiving nonvolatile pheromone signals primarily from the accessory olfactory bulb (AOB). However, that there is a contribution of volatile odor signals from the main olfactory bulb (MOB) had also been suggested. An axon guidance molecule, Neuropilin 2 (Nrp2), is known to mediate targeting of olfactory sensory neurons to the posteroventral (PV) MOB in mice. In this study, I found that Nrp2-positive ($Nrp2^{+}$) mitral cells (MCs) play crucial roles in transmitting attractive social signals from the PV MOB to the anterior part of medial amygdala (MeA). Semaphorin 3F, a repulsive ligand to Nrp2, regulates both migration of $Nrp2^{+}$ MCs to the PV MOB and their axonal projection to the anterior MeA. Gene-targeting experiments demonstrate that AOB-independent social behaviors, e.g., the suckling behavior of pups and ultrasonic vocalization of male mice, are impaired in the MC-specific Nrp2 knockout.

Table of contents

1. Introduction

The mammalian olfactory system recognizes a diverse repertoire of chemical information that induces distinct behavioral responses based on the odor qualities (Doty, 1986). Rodents have two distinct chemosensory systems: the main olfactory system, which detects volatile odors, and the vomeronasal system, which is receptive to non-volatile pheromones. In the main olfactory system, odor ligands are detected by odorant receptors (ORs) of olfactory sensory neurons (OSNs) in the olfactory epithelium (OE) (Buck and Axel, 1991). Since OSNs expressing the same type of OR send their axons to a specific target site, glomerulus (GL), and each odorant can interact with multiple OR species (Mombaerts et al., 1996; Ressler et al., 1994; Vassar et al., 1994), odor signals detected in the OE are converted into a topographic map of activated glomeruli. Odor information encoded in the olfactory bulb (OB) is then conveyed by projection neurons, mitral/tufted (M/T) cells, to various areas of the olfactory cortex (OC) to elicit odor responses (Schwob and Price, 1984; Shipley and Adamek, 1984) (Fig.1). On the other hands, the vomeronasal system detects pheromones in the vomeronasal organ (VNO). Pheromonal information is transmitted via the accessory olfactory bulb (AOB) to the medial amygdala (MeA) (Fig.1b). The MeA is known to elicit social innate behaviors such as mating and aggression (DiBenedictis et al., 2012; Lehman et al., 1980; Maras and Petrulis, 2006). However, the MeA receives social odor signals also from the main olfactory bulb (MOB). Dye-injection and pharmacological ablation experiments support this notion (Keller et al., 2006; Martel and Baum, 2007). Furthermore, some attraction behaviors mediated by the MeA are not affected in the knockout (KO) of TrpC2 (AOB-specific ion channel) (Kimchi et al., 2007; Leypold et al., 2002; Stowers et al., 2002), but impaired in the KO

of CNG-A2 (MOB-specific ion channel) (Mandiyan et al., 2005). Although these previous experiments indicate that the main olfactory system plays a critical role in inducing attractive social responses, the exact mechanism for how odor signals are correctly transmitted from the MOB to the MeA remains uncertain.

How is it then that the map information is transmitted from the OB to the OC for behavioral decisions? For olfactory map formation, OSN axons are guided to approximate locations in the OB by using different sets of axon guidance molecules (Giger et al., 1998; Imai et al., 2009; Kolodkin et al., 1997; Takeuchi et al., 2010) and the map is further refined in an activity-dependent manner (Serizawa et al., 2006). In contrast, mitral cells (MCs) are generated in the ventricular zone (VZ) at E10-13 and migrate radially, through the intermediate zone (IZ), toward the surface of the MOB (Fig.2). Because the MOB expand ventrally during development, MCs migrate tangentially to the PV regions in the MOB (Imamura et al.,2011). However, molecular mechanisms for the circuit formation of MCs are largely unknown.

How is the odor map interpreted and how are odor qualities determined for behavioral decisions? The olfactory map is not merely a projection screen that recognizes patterns to discriminate various odorants, but it is composed of functional domains that induce innate odor responses (Mori and Sakano, 2011). Previous study reported that the avoidance domain for spoiled foods and the fear domain for predator odors are separately located in the dorsal part of the OB, in D_I and D_{II} regions, respectively (Kobayakawa et al., 2007). The cortical amygdala (CoA) is reported to mediate odor information of aversive smells (Maras and Petrulis, 2006; Root et al., 2014). As for the attractive social signals, responding glomeruli are found in the posteroventral (PV) part of the OB (Fig.3). For example, male urine compounds

methylthio-methanethiol (MTMT) (Lin et al., 2005) and (Z)-e-tetradecen-1-ol (5Z-14:OH) (Yoshikawa et al., 2013) are detected by MOR83 and MOR286-3P, respectively, whose glomeruli are located in the PV OB (Duan et al., 2012). Although neural circuits have not been established for these social cues, the medial amygdala (MeA) is reported to respond to odor inputs for attractive responses (Lehman et al., 1980). I assume specific circuit links between functional domains in the OB and particular regions in the OC to induce behavioral outputs. It is also unclear whether the second-order neurons, MCs, can be divided into different subsets for specific roles and how their cell lineages are determined during development. Thus, it is quite important that the functional and structural connectivity between the MOB and the OC be elucidated.

2. Results

2.1 Nrp2$^+$ MCs in the MOB Elicit Social Attraction Responses

We have previously reported that Nrp2$^+$ OSN axons are guided from the ventral OE to the PV MOB by repulsive interactions with Semaphorin 3F (Sema3F) secreted by dorsal OSN axons (Takeuchi et al., 2010). Furthermore, a subpopulation of MCs in the PV MOB are Nrp2$^+$ (Inaki et al., 2004; Takeuchi et al., 2010). Previous study reported that the attractive odor such as conspecific urine odors are detected in the PV MOB (Duan et al., 2012). These observations suggested an intriguing possibility that Nrp2$^+$ MCs may be responsible for receiving attractive social signals from the Nrp2$^+$ glomeruli and transmitting the signals to the anterior MeA. I examined whether odor-induced social behaviors are affected in the Nrp2 cKO. MC-specific cKO mice were generated by crossing the Nrp2-floxed mice (Walz et al., 2002) with the AP2ε (immature MC marker)-Cre as a driver (Feng et al., 2009; Feng and Williams, 2003). AP2ε has restricted expression in the OB and represents the earliest known marker for the developing OB (Feng et al., 2009; Feng and Williams, 2003; Tummala et al., 2003). To demonstrate the tissue-specific activity of Cre, I crossed the AP2ε-Cre line to the ROSA-stop-lacZ mouse (Feng et al., 2009). Heavy X-gal staining was found in the MC layer in the OB (Fig. 4a), however, OSNs in the OE were devoid of staining.

Since the PV MOB is reported to be activated by urinary volatiles (Keller et al., 2006; Schaefer et al., 2001), I evaluated the response of male mice to female urine that was physically separated from the male mice so that only volatile social cues could be detected (Fig. 4b left). In the control experiment, the heterozygous littermate male was strongly attracted to the female urine, sniffing it for much longer period of time compared to that of another male's. In the male cKO of Nrp2, no difference was

observed in sniffing between the female and male urine (Fig. 4b right). I also examined whether the MTMT-induced female behaviors (Lin et al., 2005) are affected in our cKO of Nrp2. It was found that investigation times of female mice were significantly lowered in the cKO toward MTMT with castrated male urine (Fig. 4c). Interestingly, female cKO demonstrated increased attraction to the castrated male urine alone compared with controls, which may be explained by alterations of neural circuitries in the Nrp2 cKO. These results supported the idea that $Nrp2^{+}$ MOB MCs are involved in eliciting social attraction behaviors. However, one could not exclude the possibility that some diffusible urine components might have been processed by the vomeronasal organ (VNO). I, therefore, studied male-mouse ultrasonic vocalization (USV) (Nyby et al., 1977) that is regulated independently from the VNO (Kimchi et al.,2007). Male mice emit USV in response to female during courtship. USV signals emitted by resident males were compared between the cKO and heterozygous littermates in the presence of a female intruder. It was found that USV by males toward females was diminished in the MC-specific cKO of Nrp2 (Fig. 5).

I next studied suckling behavior of pups in the MC-specific cKO of Nrp2. It is known that in neonatal rabbits, nipple search is a stereotyped innate behavior regulated by maternal odor substances and independent of the AOB (Hudson and Distel, 1986). Since the VNO is not fully functional until postnatal day 10 (P10) in mice (Garrosa et al., 1998), it is unlikely that suckling behavior of pups is regulated by the VNO, but instead by the main olfactory system. In the control pups (heterozygous littermates), ~90% were able to successfully find their mother's nipples within 4 min (Fig. 6a). In contrast, less than 20% of mutant pups were able to locate the nipples. However, this difference was not due to any defect in locomotive activities. I placed pups on their

back and determined the time they spent to recover from this position (Fig. 6b). In this reflex righting test, no difference was found between the cKO and control littermates.

Previous study reported that innate fear responses induced by a fox odor, trimethyl-thiazoline (TMT), are mediated by the dorsal-region glomeruli in the MOB (Kobayakawa et al., 2007). Furthermore, the CoA is known to receive aversive information of TMT (Maras and Petrulis, 2006; Root et al., 2014). In order to determine if *Nrp2*$^{+}$ MCs are involved in eliciting fear responses to TMT, I examined TMT responsiveness in the MC-specific cKO of Nrp2. Interestingly, TMT-induced fear responses were not affected in the cKO (Fig. 6c). These observations demonstrate that the absence of Nrp2 in MOB MCs interferes with social attraction behaviors, while having no effect on the TMT-induced innate fear responses that are mediated by the dorsal MOB. Furthermore, no abnormality was found in the detection of odor substances such as α-terpinene and vanillin that activate the dorsal glomeruli (McBride and Slotnick, 2006; Oka et al., 2006). No difference was found in the habituation-dishabituation test between the cKO and heterozygous littermate mice (Fig. 7 left) even with the 10^{-5} dilution of vanillin for dishabituation (Fig. 7 right).

2.2 Nrp2^{+} MCs are Guided to the PV MOB by Sema3F

Having demonstrated that Nrp2 is essential for critical social behaviors such as USV communication, I could directly test the hypothesis that Nrp2 is involved, and potentially instructive, in neural circuit formation between the MOB and the anterior MeA. The significant changes in odor-induced social behaviors can be explained by the alterations in the neural circuitry in the Nrp2 cKO. To examine this, I first analyzed migration and distribution of Nrp2^{+} MCs in the MOB of the wild-type (WT)

mice. In the embryo, MC precursors are generated in the ventricular zone (VZ) at E10-13 and migrate radially, through the intermediate zone (IZ), to the mitral cell layer (MCL) in the MOB (Blanchart et al., 2006; Hinds, 1968). Double *in situ* hybridization, using *Pcdh21* (mature MC marker) and *Nrp2* probes, revealed that the *Nrp2* gene is expressed in a subset of MCs in the WT (Fig. 8a). Nrp2 expression gradually decreases after birth and disappears by PD14. Therefore, I attempted to analyze how the two types of MCs, *Nrp2*$^{+}$ and *Nrp2*$^{-}$, are generated in the MOB during development. Pcdh21 and AP2ε were used as developmental markers for mature and immature MCs, respectively. At E13.5, immature MCs (*AP2ε*$^{+}$) are located within the IZ, where the *Nrp2*$^{+}$ and *Nrp2*$^{-}$ cells are already separated (Fig. 8b). *In situ* hybridization revealed that not all MCs in the PV MOB are Nrp2^{+} (Fig. 8b and 8c). There may be another subset of MCs in the PV MOB, which is Nrp2^{-}. It is possible that these Nrp2^{-} MCs were originally Nrp2^{+}, but lost Nrp2 expression after migrating to the PV. My BrdU experiment indicates that both *Nrp2*$^{+}$ and *Nrp2*$^{-}$ MCs are simultaneously produced at E10-13 (Fig. 9a). At P0, when most MCs have reached the MCL, *Nrp2*$^{+}$ MCs are confined to the PV region of the MOB (Fig. 8a). As for the primary neurons, dorsal OSN axons are Nrp2^{-}, whereas the PV OSN axons are Nrp2^{+} (Fig. 9b) (Takeuchi et al., 2010). Since MCs PV tend to extend their primary dendrites perpendicularly to the nearest glomerulus, *Nrp2*$^{+}$ MC dendrites make synaptic connections with the Nrp2^{+} OSN axons in the PV MOB. This dorsal/ventral partitioning appears to provide a topographical and functional separation of the olfactory map (Kobayakawa et al., 2007; Takeuchi et al., 2010).

To specifically examine how Nrp2^{+} MCs are guided to their proper locations in the MCL, and whether Nrp2 regulates the association between OSN axons and MC

dendrites, I analyzed the Nrp2 KO mouse (Walz et al., 2002). In this total KO, a coding sequence of *Nrp2* was replaced with that of *GFP*, so that cells with activated *Nrp2* promoter could be detected with the *GFP* probe. Our studies showed that, not only the targeting of OSN axons (Fig. 10a and Fig. 11a), but also the distribution of MCs is affected in the KO mice (Fig. 10b and Fig. 11b). In contrast to the total KO, the MC-specific cKO of Nrp2 did not affect the targeting of $Nrp2^+$ OSN axons. Likewise, MC migration was not affected in the OSN-specific cKO of Nrp2 (Fig. 10b and Fig. 11b). Based on these observations, the possibility of direct crosstalk between the OSN axons and MC dendrites via Nrp2 molecules was excluded. Therefore, I focused on Sema3F, a repulsive ligand for Nrp2. Sema3F is secreted by the dorsal OSN axons to repel the ventral OSN axons and is not produced by MCs in the MOB (Takeuchi et al., 2010). To examine whether the OSN-derived Sema3F also regulates the migration of MCs, I analyzed the distribution of $Nrp2^+$ MCs in the OSN-specific cKO of Sema3F. In this cKO, distribution of $Nrp2^+$ MCs in the MOB is severely affected: $Nrp2^+$ MCs are found not only in the ventral, but also in the dorsal part of the MCL (Fig. 12b and Fig. 13b). In the same Sema3F cKO, $Nrp2^+$ OSN axons are also defasciculated in the glomerular layer (GL) (Fig. 12a and Fig. 13a). These phenotypes are similar to those observed in the total KO of either Sema3F or Nrp2 (Figs 10-13). I performed these targeting experiments at both E18 and P0 and obtained basically the same results. However, signals were clearer at E18 than P0 in the hybridization experiment probably due to the differences in transcription levels of *Nrp2*. In contrast, I obtained better staining at P0 than E18 in the immunohistochemistry. Taken altogether, I conclude that for proper matching to occur, OSN-derived Sema3F in the

dorsal MOB regulates both targeting of Nrp2$^+$ OSN axons and migration of *Nrp2*$^+$ MCs to the PV MOB.

2.3 Nrp2$^+$ MCs Target Their Axons to the Anterior MeA

To study a specific function of *Nrp2*$^+$ MCs in inducing social attraction behaviors, I next analysed their axonal projection and arborization in the OC. MCs send their axons to various brain regions by following the lateral olfactory tract (LOT) (Devor, 1976; Shipley and Adamek, 1984; Suarez et al., 2012; Treloar et al., 2003; Yoshihara et al., 1999) (Fig. 14a right). Since Nrp2 expression was not sufficiently strong for tracing axons by immunostaining, I developed a transgenic (Tg) mouse in which the fluorescent reporter protein, EYFP, was expressed in *Nrp2*$^+$ MCs. To do this, I generated Tg mice carrying the transgene, *pcdh21-lacZ-STOP-tauEYFP*, in which the Cre-inducible *tauEYFP* gene was expressed with the *Pcdh21* promoter (Fig. 14a). The *lacZ* gene was introduced into the construct to monitor the *Pcdh21* promoter activity (Fig. 15a left). Four independent mouse lines, that successfully expressed the *lacZ* gene in MCs, were obtained. While the *Pcdh21* promoter is usually active in both the MOB and the AOB, in one of our four mouse lines, the transgene was activated only in the MOB and not in the AOB (Fig. 15a right). Signals of β-gal seen around the AOB are MC axons passing by from the MOB. This mouse line proved quite useful for analyzing MOB MCs for axonal projection separately from AOB counterparts. To activate the *EYFP* gene specifically in the *Nrp2*$^+$ MCs of the MOB, the mouse was then crossed with another Tg mouse containing the *Nrp2-Cre*, where Cre-recombinase was induced by the *Nrp2* promoter (Fig. 14a). As expected, EYFP signals were detected only in the PV-region MCs, but not in the dorsal ones (Fig. 15b). This Tg mouse also

allowed us to trace the trajectory of axonal projection of *Nrp2*$^{+}$ MCs by immunostaining EYFP.

MCs in the MOB have been reported to project their axons to various regions of the OC, including the anterior olfactory nuclei (AON), piriform cortex (PIR) and CoA (de Olmos et al., 1978; Dulac and Torello, 2003; Scalia and Winans, 1975; Yoshihara et al., 1999). Consistent with these previous reports, EYFP^{+} axons are found in the superficial layer of these nuclei (Fig. 14b left). Staining signals of EYFP are uniformly distributed throughout these areas and no clustering of staining signals is observed. Interestingly, EYFP^{+} axons are detected in the MeA (Fig. 14b left), but are negative for OCAM, a marker for dorsal-region MCs (Treloar et al., 2003) (Fig 14b right). Here, I analyzed the cortical projection at P14, because MC targeting is completed at P14. However, OCAM staining was performed at P0, because OCAM expression decreases after birth. I also observed that the EYFP^{+} region is positive for Nrp1, a marker for MOB MCs (Fig 16). Double ISH confirmed that *Nrp1* is expressed in the Nrp2^{+} MCs (Fig. 16b). These results clearly demonstrate that Nrp2^{+} MCs in the MOB connect the PV-region MOB and anterior MeA.

2.4 Trans-Synaptic Labeling of MCs in the MOB

To examine whether anterior MeA neurons selectively receive afferent projections from the PV MOB, I performed mono-synaptic labeling with the recombinant rabies virus (RV), which transmits across synapses in a retrograde direction (Wickersham et al., 2007). For the labeling of MCs, I used recombinant virus RV-ΔG-EGFP-EnvA that requires target cells to express avian receptor protein TVA and glycoprotein G for its selective infection, as well as mono-synaptic transmission (Fig. 17a). I first

injected adeno-associated virus (AAV) into the anterior side of MeA to complement TVA and glycoprotein G (Fig. 17b left). After 2 weeks, RV-ΔG-EGFP-EnvA was injected into the same MeA region to selectively infect neurons expressing the TVA receptor. After 10 more days, serial sections of the entire MeA were analyzed to confirm that the neurons infected with the AAV and RV were indeed confined to the MeA (Fig. 17b left). I then examined the locations of EGFP-labeled MCs that were retrogradely infected with the RV. Eighty-one starter-cells gave rise to 179 labeled MCs, 150 of which were specifically found in the PV MOB (Fig. 17b right) suggesting that the MeA receives biased inputs from the PV-MOB. For a control experiment, I injected the AAV and RV into the PIR where 478 labeled MCs were generated from 98 starter-cells in the PIR (Fig. 17c left). No special preference was found in their locations in the MOB (Fig. 17c right): EGFP-positive MCs are distributed randomly in the MOB as reported (Miyamichi et al., 2011). These observations further support the idea that the anterior MeA receives MC projection from the MOB from the PV region.

2.5 Targeting of Nrp2^{+} MCs is also Regulated by Sema3F

How do the *Nrp2*$^{+}$ MCs project their axons from the PV MOB to the anterior MeA? To examine the possibility that Nrp2 expressed by MCs plays a critical role in guiding axons, the MC-specific cKO of Nrp2 was analyzed at P14 for MC projection from the MOB. Since Nrp2 signals are hardly detected at this stage, anti-Nrp1 antibodies were used to detect MOB MC axons. Staining signals of Nrp1, a marker for MOB MCs, are severely reduced in the MeA of the Nrp2 KO (Fig. 18), although signal levels are not changed in other OC regions (Fig. 19). This observation demonstrates that the lack of Nrp2 leads to the dramatic decrease in the number of MC axons

projecting from the MOB to the anterior MeA. A similar reduction is also found in the total KO of Sema3F, a repulsive ligand for Nrp2 (Fig. 18). It is interesting that the axonal projection of *Nrp2*$^{+}$ MCs is not affected by the OSN-specific cKO of Sema3F (Fig. 18 and Fig. 20), where the *Nrp2*$^{+}$ and *Nrp2*$^{-}$ MCs are not properly segregated within the MOB. This observation suggests that axonal projection of MCs to the anterior MeA takes place independent of their locations in the MOB. In the Sema3F total KO, MCs in the AOB also fail to converge to the MeA and mistarget to the CoA (Fig. 21). Since Sema3F is detected in the cortical regions surrounding the MeA (Fig. 22), *Nrp2*$^{+}$ MC axons are likely guided to the MeA by repulsive interactions with Sema3F in the embryonic OC. Taken altogether, our results indicate that Nrp2 plays a dual instructive role in regulating MC migration within the MOB and in guiding axons of PV-region MCs to the anterior MeA through repulsive interactions with Sema3F expressed in the dorsal MOB and outside regions of the MeA, respectively.

2.6 In Utero Electroporation of the Human *Nrp2* Gene

Although I could demonstrate an essential role of Nrp2 in linking the PV MOB and anterior MeA, it was not clear whether the activation of *Nrp2* is sufficient or any additional genes need to be activated in MCs to induce the circuit formation. In order to examine how much is regulated by Nrp2, we performed gain-of-function experiments by using *in utero* electroporation. A plasmid vector containing *EGFP* cDNA was introduced into the WT embryonic OB with or without the human *Nrp2* (*hNrp2*) cDNA. As reported previously (Imamura and Greer, 2015), when the *EGFP* was introduced alone at E11, immunostaining signals for EGFP were equally distributed in both the dorsal and ventral regions of the MCL at P0 (Fig. 23a). In contrast, when the *hNrp2*

gene was co-transfected with *EGFP*, $EGFP^+$ cells were confined to the PV region in the MOB, as observed in MCs expressing endogenous *Nrp2* (Fig. 23a). $EGFP^+$ cells were mostly positive for MC markers, Tbr1, Tbr2, and Tbx21 (Fig. 23b). This observation shows that constitutive expression of the exogenous *Nrp2* gene is sufficient to bring MOB MCs to the PV region, even those that would normally remain in the dorsal MOB.

We then analysed axonal projections of MCs in the electroporated WT mice (Fig. 24). EGFP signals were not strongly found in the MeA when the *EGFP* was electroporated without *hNrp2* (Fig. 24a). In contrast, EGFP signals were significantly increased in the anterior MeA at P0, when the *hNrp2* was co-transfected with *EGFP* (Fig. 24b). These experiments indicate that ectopic expression of *hNrp2* can promote, not only the migration of MCs to the PV MOB, but also their axonal projection to the anterior MeA. It is interesting that staining signals for OCAM, a dorsal-MOB MC marker, were detected in the anterior MeA on the ipsilateral side of the MOB electroporated with *hNrp2* cDNA (Fig. 24b). This indicates that constitutive expression of exogenous Nrp2 alone can instruct axonal projection to the anterior MeA even in the dorsal-lineage ($OCAM^+$) MCs that do not normally send their axons to the anterior MeA. Taken together, these observations clearly demonstrate that activation of *Nrp2* is not only necessary but also sufficient to instruct circuit formation of MCs from the PV MOB to the anterior MeA. *In utero* electroporation experiments were performed by Dr. Fumiaki Imamura.

3. Discussion

In the present study, I analyzed roles of *Nrp2*$^{+}$ MCs in generating the neural circuit for attractive social responses. We previously reported that Sema3F secreted by Nrp2^{-} dorsal OSN-axons directs late-arriving Nrp2^{+} OSN axons to the PV MOB (Takeuchi et al., 2010). The same dorsal-OSN-derived Sema3F was found to guide *Nrp2*$^{+}$ MCs from the VZ to the PV region of MOB. This coordinated regulation of OSN projection and MC distribution appears to be key for functional pairing of OSN axons and MC dendrites in the MOB. I further examined targeting of *Nrp2*$^{+}$ MCs localized to the PV MOB. In a previous report (Kang et al., 2009), dye-injection experiments indicated that the MeA receives MC inputs not only from the AOB, but also from the MOB. By using fluorescent tags, I found that *Nrp2*$^{+}$ MCs send their axons to the anterior portion of MeA. Furthermore, retrograde virus-tracing revealed that *Nrp2*$^{+}$ MCs in the PV MOB do indeed form synapses with MeA neurons.

Our gain-of-function (*in utero* electroporation) and loss-of-function (KO) experiments demonstrate that Nrp2-Sema3F repulsive interactions are essential, not only for guiding *Nrp2*$^{+}$ MCs to the PV MOB, but also for instructing their axons to the anterior MeA (Fig. 25). In the *in utero* electroporation experiment, MCs expressing hNrp2 with EGFP are not only guided to the PV MOB, but also instructed to send their axons to the anterior MeA. In the electroporated mice, the EGFP^{+} (hNrp2^{+}) region in the anterior MeA became positive for the dorsal MC marker, OCAM. These results demonstrate that ectopic expression of hNrp2 in the mouse MCs is sufficient to instruct their circuit formation to the anterior MeA even in dorsal-lineage MCs. It will be interesting to study whether these transfected neurons form functional circuits receiving OSN input from the OB and making synaptic connections to the anterior MeA.

In the Nrp2 total KO and MC-specific cKO, signals of MC axons projecting from the MOB are significantly reduced in the anterior MeA, and a similar phenotype is observed in the Sema3F total KO. MCs that were supposed to project to the MeA may reroute their axons targeting to other areas in the OC or simply do not survive during development. Since Sema3F is expressed in the cortical regions surrounding the MeA during early embryonic development, *Nrp2*$^{+}$ MC axons are likely driven to the MeA by repulsive interactions with Sema3F expressed just outside their trajectory. It seemed puzzling that *Nrp2*$^{+}$ MCs targeted their collaterals to the Sema3F^{+} areas in the OC at later stages of development. However, this can be explained by the temporal regulation of *Nrp2* and *Sema3F* expression: Both *Nrp2* and *Sema3F* are expressed at embryonic stages (E12-18), but disappear later on when collateral extension starts to occur. It has been reported that the D-V topography in the OB is roughly correlated with that in the anterior olfactory nucleus pars externa (AONpE) but not in the PIR (Ghosh et al., 2011; Miyamichi et al., 2011; Sosulski et al., 2011; Yan et al., 2008). Furthermore, incoming odor signals in the CoA are mostly from the dorsal OB (Miyamichi et al., 2011; Sosulski et al., 2011). Keeping these previous observations in mind, I closely analyzed the secondary projection of Nrp2^{+} MCs to the AON, PIR, MeA, and CoA. I found that Nrp2^{+} MCs in the PV OB preferentially target their axons to the anterior MeA, although they send their axons to the AON, PIR and CoA as well.

MCs exhibit a protracted waiting period before sending their collateral branches to the target. It has been reported that the target OC in culture becomes accessible to MC fibers at E16.5 during development (Hirata and Fujisawa, 1999). Innervation in the central areas is completed by PD15. First collaterals are extended towards the AON and PIR at E16.5, and innervation to the OT is completed after birth (Hirata and

Fujisawa, 1999; Walz et al., 2006). Despite these previous studies, timing of innervation to the MeA was still unclear. Our study demonstrates that Nrp2 instructs targeting of ventral MCs to the MeA. During development, Nrp2 is expressed in the ventral MCs at embryonic stages, but disappears by PD14. It is likely that innervation to the MeA occurs at embryonic stages.

The MeA is known to process non-volatile pheromone signals, detected by the VNO, to induce innate social behaviors, such as mating, conspecific recognition and fear responses (Choi et al., 2005; DiBenedictis et al., 2012; Hong et al., 2014; Lehman et al., 1980; Maras and Petrulis, 2006). Previous dye-injection experiments suggested that the MeA also receive MOB inputs in the anterior regions (Kang et al., 2009). Furthermore, a surgical lesion to the anterior MeA of the hamster has been shown to abolish the males' preference for female urine over that of male's (Maras and Petrulis, 2006). Our present study demonstrates that it is the $Nrp2^{+}$ subset of MCs that sends attractive social inputs from the PV MOB to the anterior MeA. In the MC-specific cKO of Nrp2, AOB-independent social behaviors are affected. For example, pup suckling and male vocalization are impaired in the cKO. It is generally accepted that the AOB detects non-volatile social cues to induce various innate behaviors, whereas the MOB detects volatile odor ligands (Stowers and Marton, 2005). During evolution, the mammalian olfactory system rapidly expanded the MOB structure to accommodate greater numbers of glomeruli for classII ORs devoted to volatile odorants in the ventral region (Niimura, 2009). It is probable that the MOB developed a subset of $Nrp2^{+}$ MCs that allowed axons to project to the MeA using the Nrp2/Sema3F guidance system, similar to the AOB. This may have conferred the evolutionary advantage of detecting volatile social cues from distances. It is quite possible that the main olfactory system

governs attractive social responses, even in the human whose VNO no longer has any function and vomeronasal-receptor genes have all become pseudogenes (Meisami and Bhatnagar, 1998; Meredith, 2001).

It is rather surprising that activation of a single axon guidance gene, *Nrp2*, in immature MCs is sufficient to instruct their neural circuit formation to the anterior MeA. Our present study clearly demonstrates that *Nrp2*$^{+}$ MCs in the PV MOB play a critical role in inducing attractive social responses. These findings demonstrate a close correlation between functional domains in the MOB and specific regions in the OC (Fig. 25d). I assume that this is accomplished by gathering glomeruli with the same behavioral quality to a restricted area (functional domain) in the MOB. It is also important for MCs to ensure that the olfactory inputs with the same odor quality, regardless of their chemical nature, are transmitted to a specific region in the OC so that they could induce the same type of outputs. For attractive social responses, Nrp2 is a key determinant for connecting the PV MOB and anterior MeA by using a specific subset of MCs.

It is quite possible that this kind of circuit formation observed in MCs, which is directed by a distinct set of guidance molecules, is a general rule that is applicable to other innate odor responses. For example, fear to predators' smell and avoidance to spoiled food odors are induced by activation of glomeruli located in the avoidance (D_I) and fear (D_{II}) domains in the MOB, respectively (Kobayakawa et al., 2007). Furthermore, the CoA is reported to play an important role in inducing aversive responses to fox odor TMT (Root et al., 2014). It will be interesting to determine which axon guidance system is responsible for establishing the MC circuits connecting the dorsal MOB and CoA. In summary, it has become clear in the present study that

activation of a single guidance gene, *Nrp2*, could determine a functional lineage of MCs and is sufficient to instruct circuit formation between the MOB and OC for attractive social behaviors.

4. Conclusions

In this paper, I found that a subset of mitral cells (MCs) that are Neuropilin 2-positive ($Nrp2^{+}$), plays a critical role in transmitting attractive social signals from the PV MOB to the anterior MeA (aMeA). Nrp2 co-regulates axonal projection of OSN and cell arrangement of MC in cell-autonomous manner. Semaphorin3F (Sema3F), a repulsive ligand for Nrp2, from the dorsal OSN regulates both targeting of $Nrp2^{+}$ OSN axons and migration of *Nrp2*$^{+}$ MCs to the PV MOB. Since MC project their primary dendrites to the nearest glomerulus, $Nrp2^{+}$ OSN axons and $Nrp2^{+}$ MC make synaptic connections.

I also found that Sema3F regulate $Nrp2^{+}$ MC projection to the aMeA. In the Sema3F KO, the projection of $Nrp2^{+}$ MC to the aMeA severely reduced, although the projection to the other OC regions are not changed. Furthermore, *in utero* electroporation demonstrates that activation of the *Nrp2* gene in MCs is sufficient to instruct circuit formation from the PV MOB to the anterior MeA.

In the MC-specific conditional KO (cKO) of Nrp2, both circuit formation of $Nrp2^{+}$ MCs and odor-induced social attraction behaviors are impaired. Ultrasonic vocalizations (USV) by males towards females was diminished in the MC-specific cKO of Nrp2. However, fear responses to TMT (fox odor) were not affected in the cKO.

These results indicate that repeated use of same guidance molecules (Nrp2-Sema3F) regulate circuit formation from peripheral to higher brain center. And this circuit relay attractive social signals from PV MOB to the aMeA.

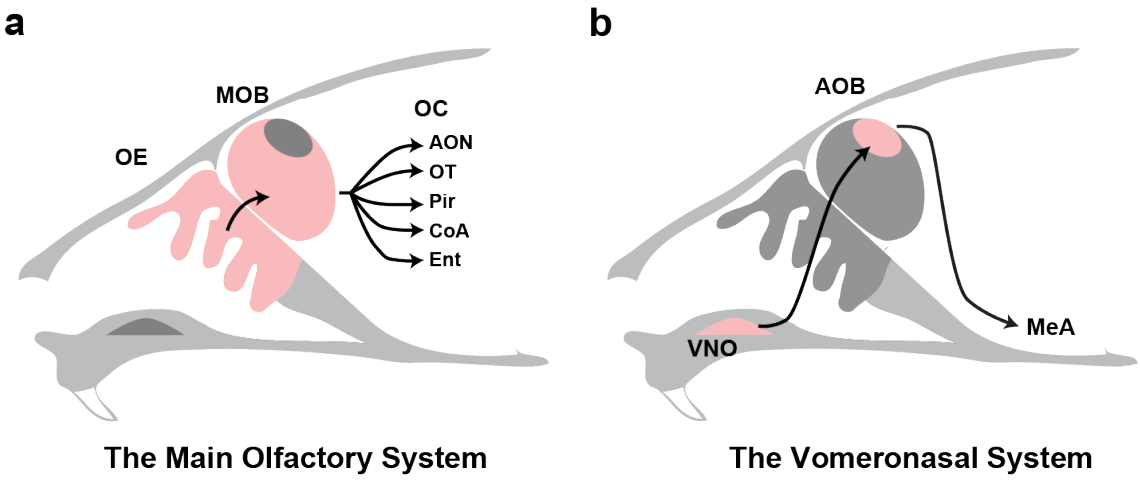

Fig.1 The Mouse Olfactory System

(a) The main olfactory system. Volatile Odorants are detected by the olfactory sensory neuron in the olfactory epithelium (OE). The odor information is transmitted to the olfactory bulb (OB), which relays the information to the olfactory cortex (OC).

(b) The vomeronasal system. Pheromones are detected by the vomeronasal organ (VNO). The signals are transmitted via the accessory olfactory bulb (AOB) to the medial amygdala (MeA)

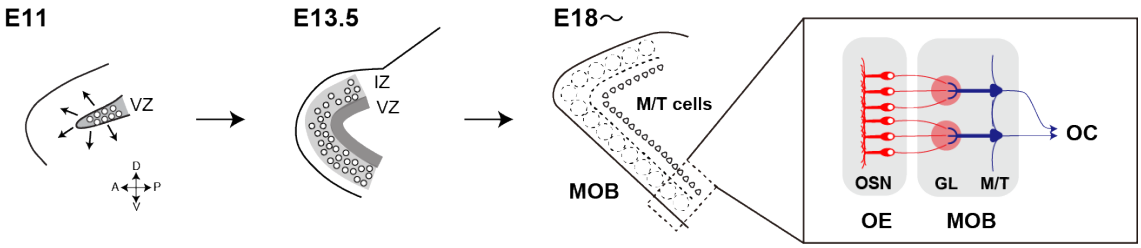

Fig.2　Development of the MOB

M/T cells are supplied from the ventricular zone (VZ) in embryo and migrate radially to the MOB surface through the intermediate zone (IZ). M/T cells extend their primary dendrite vertically to the glomerulus and connect with OSN axons.

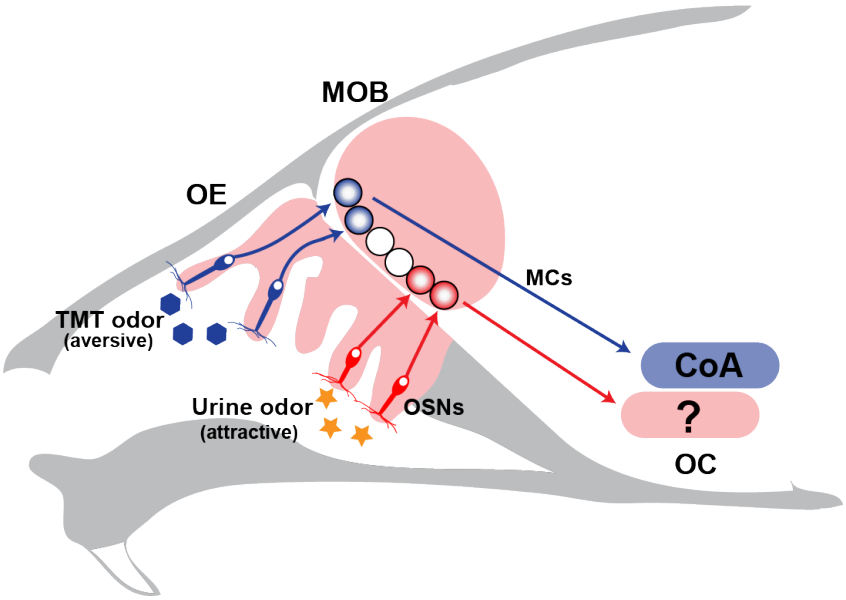

Fig.3　Circuit formation of the main olfactory system

Aversive odor (TMT) recognized by the dorsal region in the MOB.　Dorsal M/T cells project their axons to the cortical amygdala (CoA).　In contrast, ventral MOB is activated by attractive odor (urine).

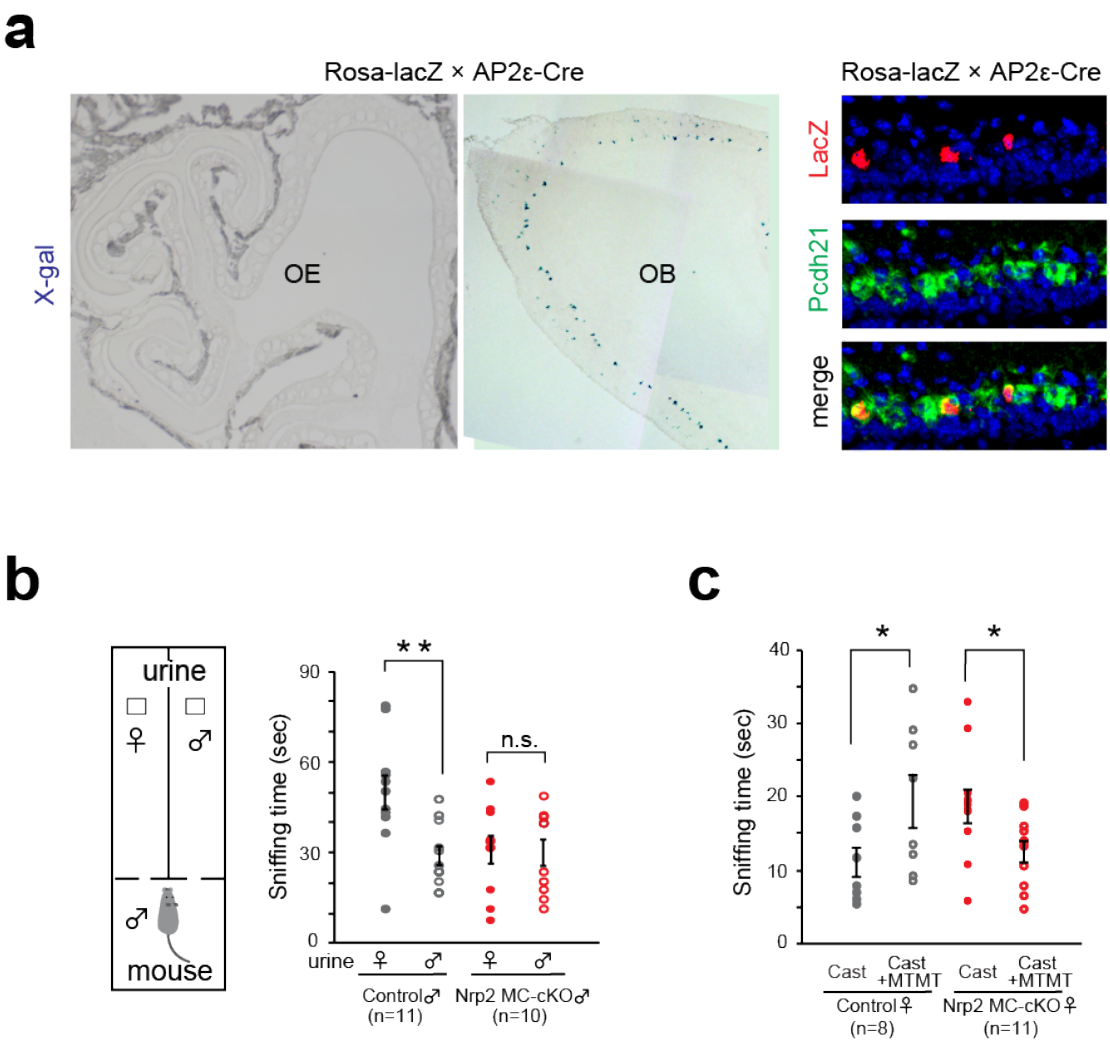
a
Rosa-lacZ × AP2ε-Cre
Rosa-lacZ × AP2ε-Cre
X-gal
OE
OB
LacZ
Pcdh21
merge
b
urine
mouse
Sniffing time (sec)
urine
Control♂
(n=11)
Nrp2 MC-cKO♂
(n=10)
n.s.
c
Sniffing time (sec)
Cast
Cast +MTMT
Control♀
(n=8)
Nrp2 MC-cKO♀
(n=11)

Fig. 4 Innate attractive behaviors in the MC-specific cKO of Nrp2.

(a) Detection of the *AP2ε* promoter activity (left). The Tg AP2ε-Cre mouse was crossed with the ROSA-shutter-lacZ mouse for Cre-mediated *lacZ* induction. Coronal sections of the OE and a parasagittal section of the OB at P14 were analyzed by X-gal staining. MCs were stained blue in the OB. $LacZ^{+}$ $PCdh21^{+}$ cells in the MCL (right). Parasagittal OB section were immunostained with antibodies against β-gal and Pcdh21. **(b)** The male attractive behavior toward female urine. A piece of filter paper spotted with 60 μl of male or female urine was presented to the male cKO or heterozygous littermate as a control. Sniffing time duration was measured within 5 min after presenting the filter paper. Although the control male spent longer times sniffing female urine, the cKO male did not show any preference. Data are presented in mean ±SE. **P< 0.01, n.s.: not significant (Student's *t* test). **(c)** The female attractive behavior toward MTMT. A piece of filter paper spotted with 50 μl of castrated male urine or castrated male urine with 20 ppb MTMT was presented to the female cKO. Sniffing time duration was measured within 5 min after presenting the filter paper. Data are presented in mean ±SE. *P< 0.05 (Student's *t* test).

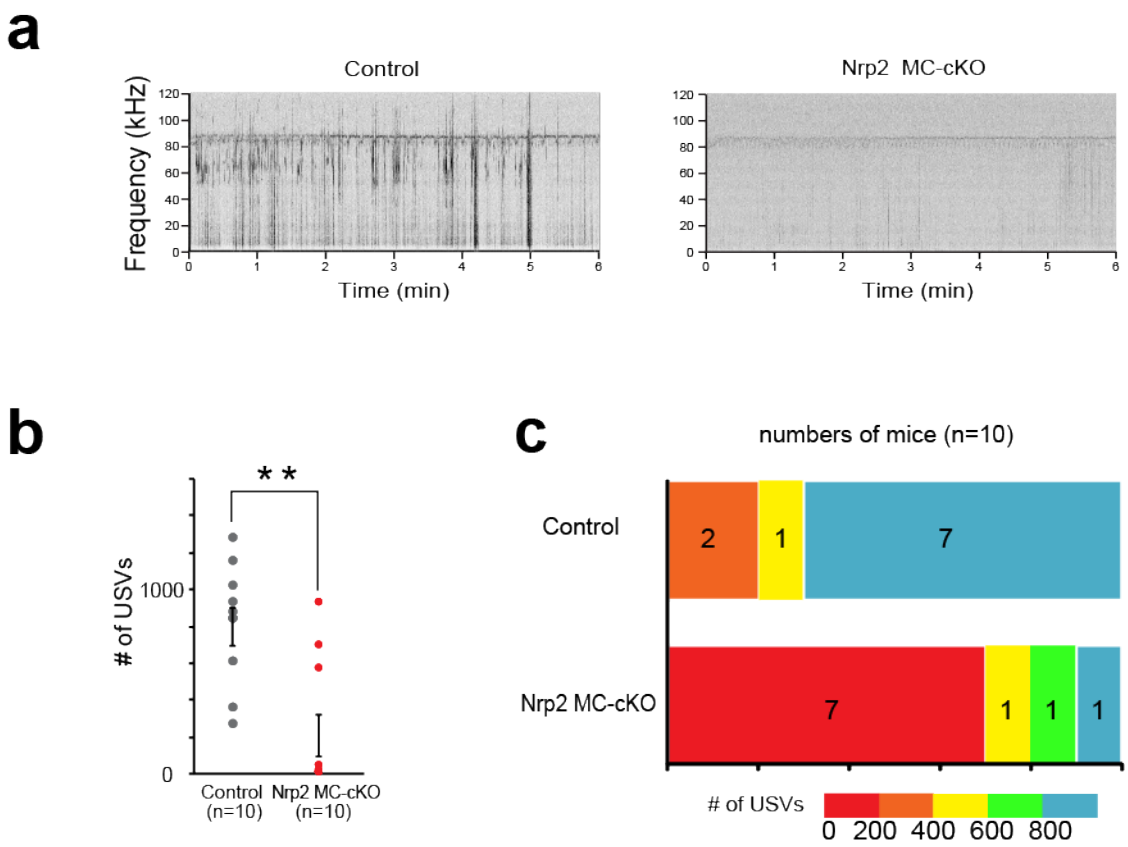

Fig. 5 Ultrasonic vocalizations in the MC-specific cKO of Nrp2.

(a) Spectrograms of ultrasonic vocalizations (USVs). USV signals emitted by resident males are compared between the cKO and heterozygous littermates in the presence of a female intruder. The intruder female was introduced into the cage for 6 min in each trial. Very few signals are detected in the cKO male. **(b)** Comparison of numbers of USV signals elicited by male mice in the presence of a WT female. USV is significantly reduced in the cKO. Data are presented in mean ±SE. **P< 0.05 (Wilcoxon signed-rank test). **(c)** Distribution of numbers of male USV. USV was counted in the presence of a female intruder for duration of 6 min in each experiment.

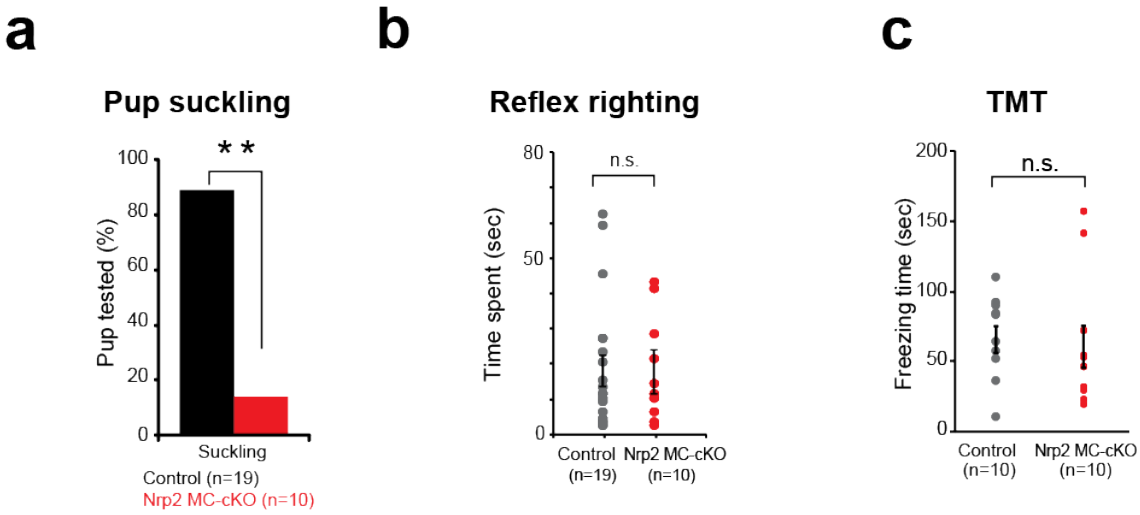

Fig. 6 Innate social behavior in the MC-specific cKO of Nrp2

(a) Suckling behavior in the Nrp2 MC-cKO pups. Lactating female mice were anesthetized and laid sideways, exposing their nipples toward pups. Pups were fasted for 4 hr prior to the experiment and placed ~1 cm away from the females' nipples. The time to find nipples for suckling was measured within 4 min. Most cKO pups failed to find nipples within 4 min. (n=19 for the control, n=10 for the MC-specific cKO of Nrp2). **P<0.01 (Z-test). (**b**) Locomotor abilities test. Mice were placed on their back. The time they spent to recover from this position, to being upright and on four paws, was measured (reflex righting). No difference was found between the cKO and heterozygous littermates in their recovery time lengths. **(c)** Fear responses to a predator's odor. A piece of filter paper spotted with 10 μl of undiluted TMT was presented to the cKO and heterozygous littermate as a control. Freezing time lengths were measured during the 10 min exposure to TMT. n.s.: not significant (paired *t* test). Data are presented in mean ±SE.

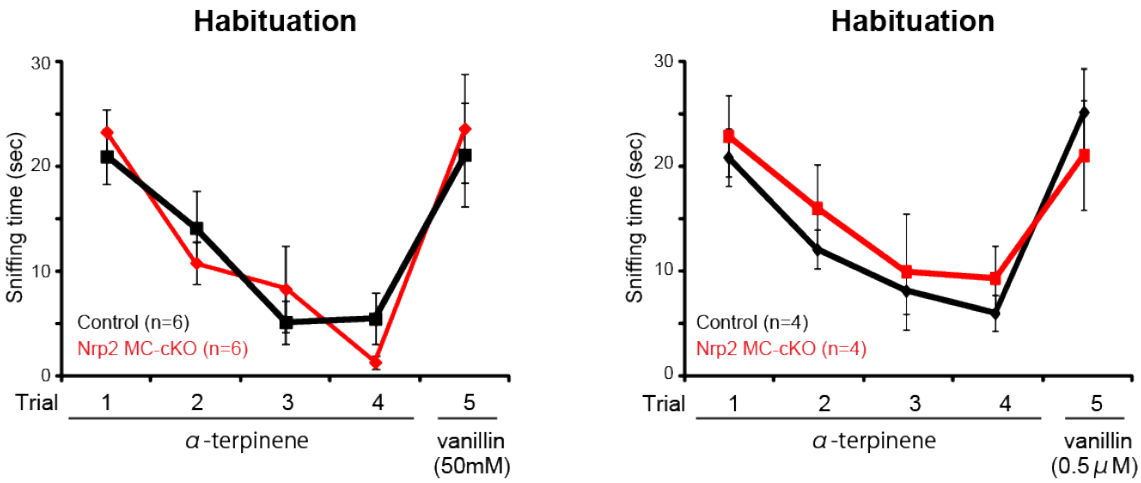

Fig. 7 Odor sensing is not affected by the MC-specific cKO of Nrp2.

Habituation-dishabituation test. In this test, α-terpinene was presented in four consecutive trials for duration of 1 min. The inter-trial interval was 10 min. Then, a novel odor vanillin (50 mM or 0.5 μM) was presented. Habituation is defined by a progressive decrease in sniffing towards the repeated presentation of the same odor stimulus. Dishabituation is defined by reinstatement of sniffing when the novel odor is presented. Graphs demonstrate amounts of time that the male cKO and control littermates spend on sniffing a piece of filter paper spotted with vanillin or α-terpinene. Trials with vanillin as the repetitive odor and α-terpinene as the novel odor yielded similar results. No difference is found between the cKO and control mice. Error bars are ±SE. Error bars are ±SE. n.s.: not significant (Student's *t* test).

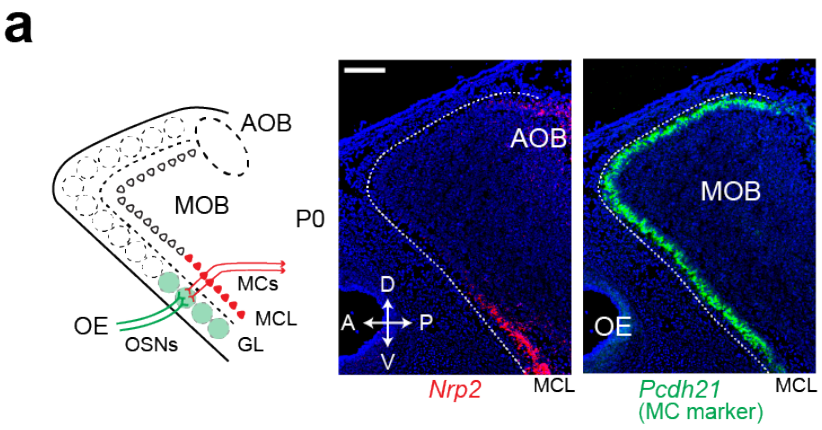
a
AOB
MOB
MCs
MCL
OE
OSNs
GL
P0
AOB
D
A
P
V
Nrp2
MCL
MOB
OE
Pcdh21
(MC marker)
MCL

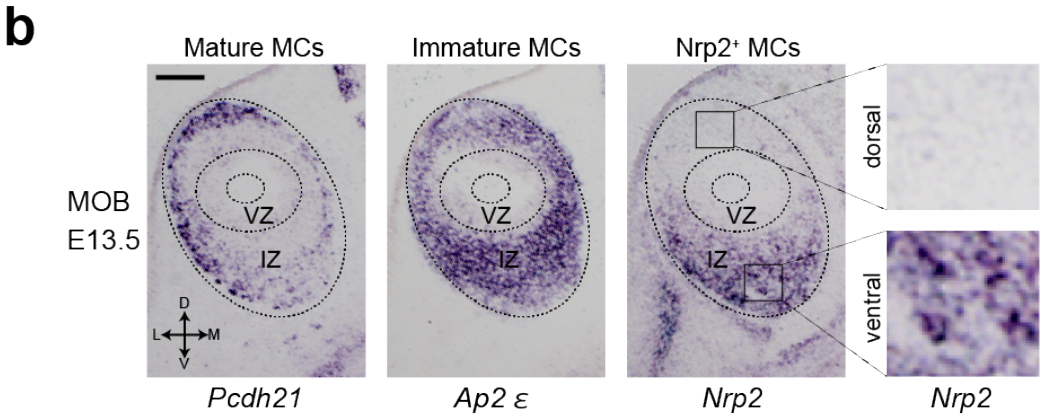
b
Mature MCs
Immature MCs
Nrp2+ MCs
MOB
E13.5
VZ
IZ
D
L
M
V
dorsal
ventral
Pcdh21
Ap2 ε
Nrp2
Nrp2

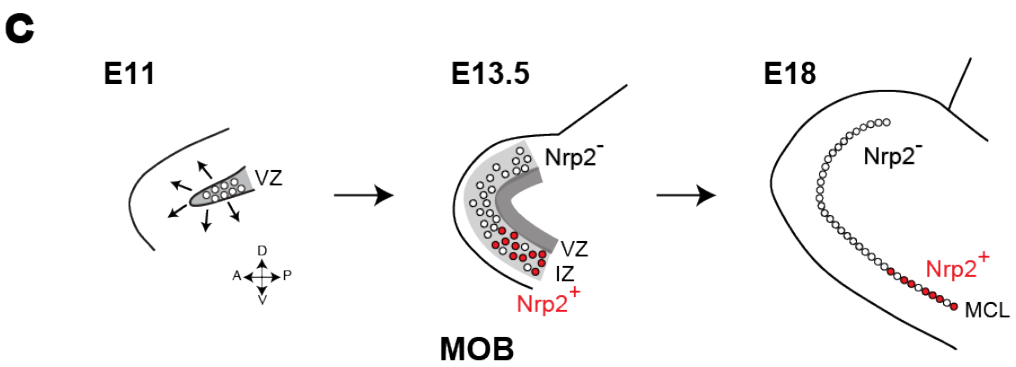
c
E11
E13.5
E18
VZ
D
A
P
V
Nrp2-
VZ
IZ
Nrp2+
Nrp2-
Nrp2+
MCL
MOB

Fig. 8 Distribution of Nrp2 in the MCL of the MOB.

(a) Detection of *Nrp2* transcripts in the ventral-region mitral cells (MCs). Parasagittal MOB sections (P0) were hybridized with *Pcdh21* (MC marker) and *Nrp2* probes. n=5. *Nrp2* is expressed in the MC layer (MCL), high in the ventral and low in the dorsal region. *Nrp2*$^{+}$ signals seen in the PD region represent Nrp2^{+} MCs in the AOB**.** A schematic diagram of the mouse MOB is shown in the left. **(b)** Distribution of *Nrp2*$^{+}$ mitral cells (MCs) in the embryonic MOB. Serial MOB sections at E13.5 were hybridized with the *Nrp2*, *AP2ε* (immature MC marker) and *Pcdh21* (mature MC marker) probes. During development, MCs are generated in the ventricular zone (VZ) and migrate radially to the MOB surface through the intermediate zone (IZ). **(c)** Schematic diagrams of MC migration during development. In the embryo, MC precursors are generated in the VZ and migrate radially to the surface of MOB (left). Nrp2^{+} and Nrp2^{-} immature MCs are segregated in the IZ (middle). Nrp2^{+} and Nrp2^{-} MCs are distributed in the posteroventral and dorsal MCL, respectively. VZ, ventricular zone; IZ, intermediate zone; MCL, mitral cell layer.

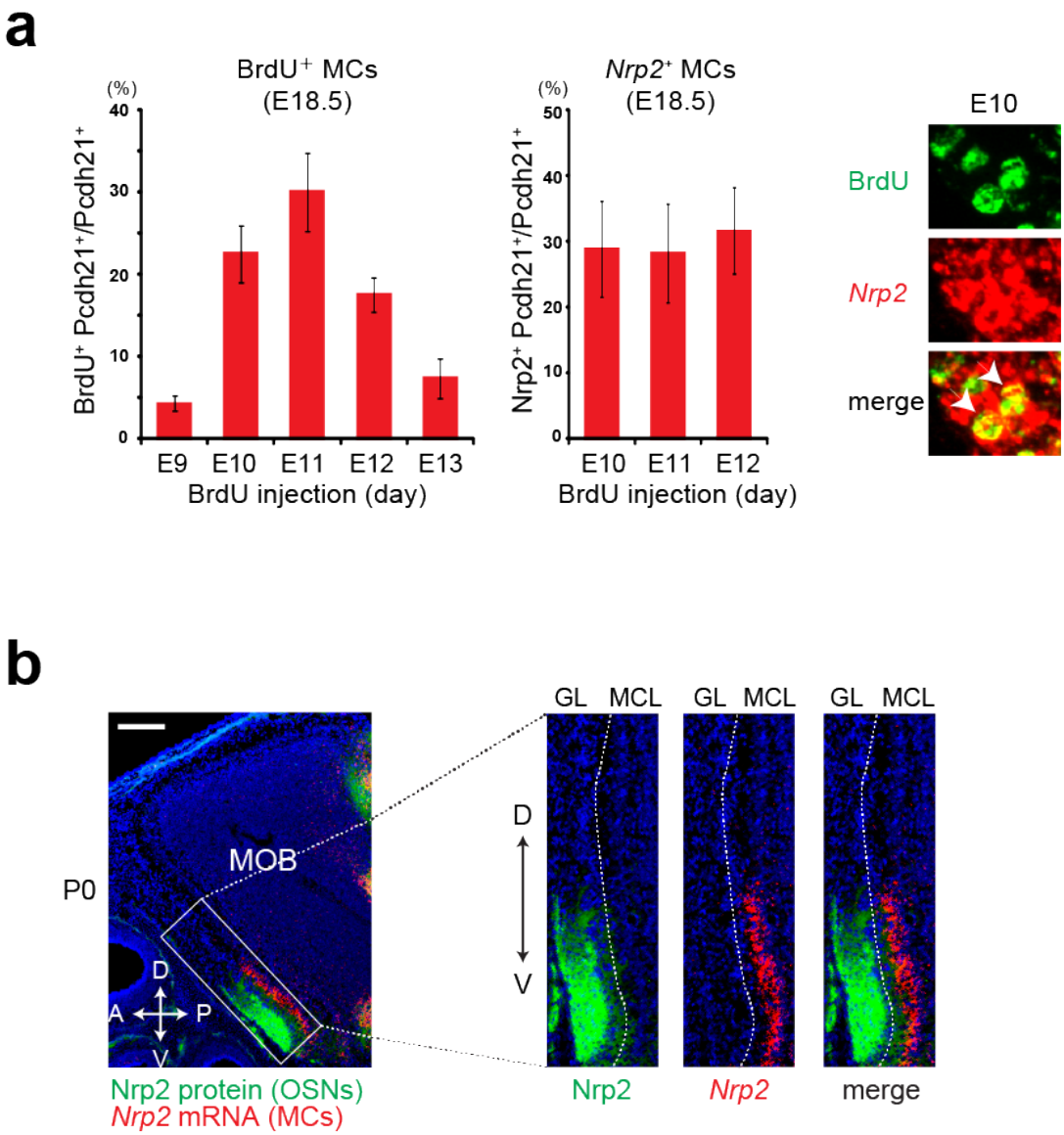
a
BrdU+ MCs
(E18.5)
(%)
BrdU+ Pcdh21+/Pcdh21+
E9 E10 E11 E12 E13
BrdU injection (day)
Nrp2+ MCs
(E18.5)
(%)
Nrp2+ Pcdh21+/Pcdh21+
E10 E11 E12
BrdU injection (day)
E10
BrdU
Nrp2
merge
b
P0
MOB
D
A
P
V
Nrp2 protein (OSNs)
Nrp2 mRNA (MCs)
GL MCL
GL MCL
GL MCL
D
V
Nrp2
Nrp2
merge

Fig. 9 Developmental expression of *Nrp2*.

(a) Generation of *Nrp2*$^{+}$ MCs during embryonic development. BrdU was injected into pregnant mice at E9, 10, 11, 12 and 13. At E18.5, MOB sections were immunostained with anti-BrdU antibodies and hybridized with the *Nrp2* probe. Ratios (%) of MCs labeled with BrdU at indicated time points are shown (left). Percentages of *Nrp2*$^{+}$ MCs labeled with BrdU are compared at E10, 11 and 12 (middle). BrdU^{+} and *Nrp2*$^{+}$ MCs injected at E10 are shown in the right. A scale bar is 200 μm. Data are presented in mean ±SE. **(b)** Distribution of Nrp2 protein and *Nrp2* transcripts in the MOB. MOB sections at P0 were immunostained with anti-Nrp2 antibodies or hybridized with the *Nrp2* probe. Nrp2 and *Nrp2* signals are distributed in parallel along the D-V axis in the glomerular layer (GL) and MCL, respectively. Enlarged photos are shown in the right. n=5.

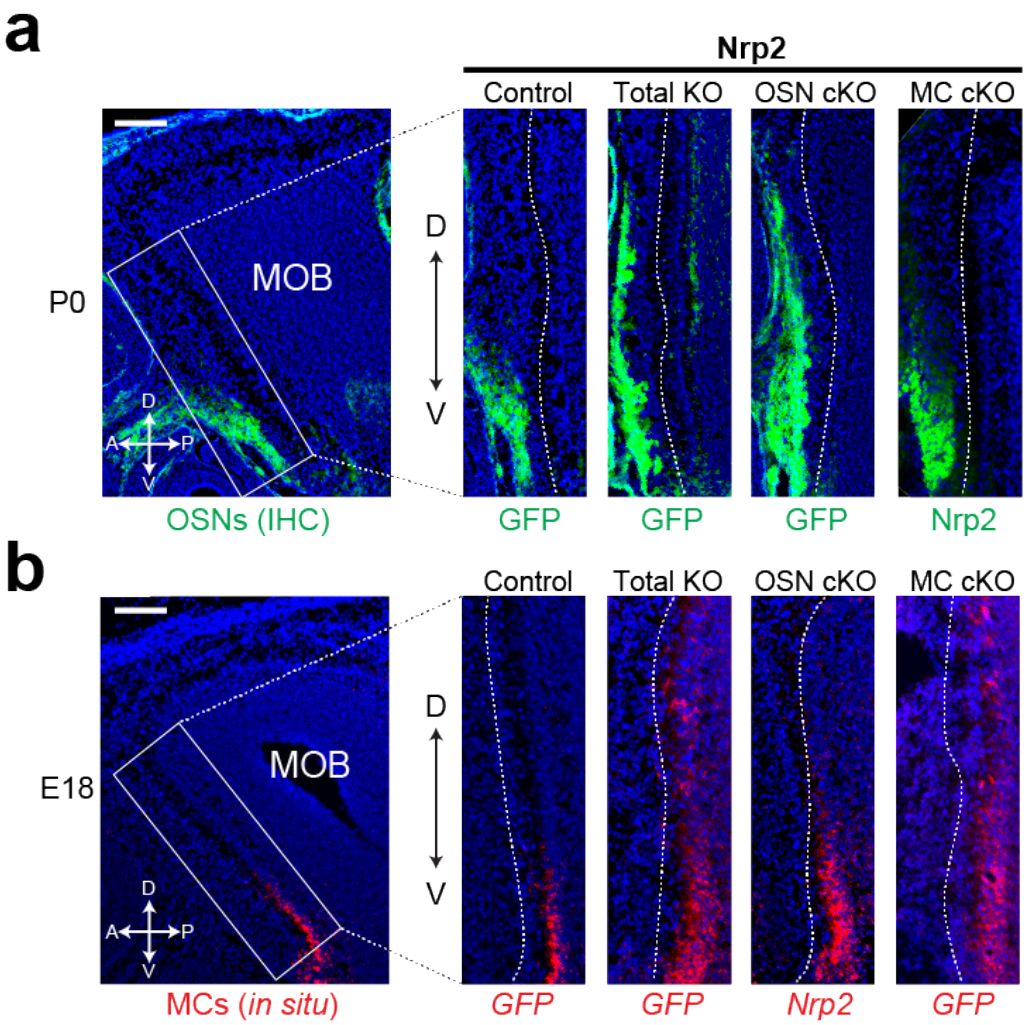
a
Nrp2
Control
Total KO
OSN cKO
MC cKO
P0
MOB
D
A
P
V
D
V
OSNs (IHC)
GFP
GFP
GFP
Nrp2
b
Control
Total KO
OSN cKO
MC cKO
E18
MOB
D
A
P
V
D
V
MCs (in situ)
GFP
GFP
Nrp2
GFP

Fig. 10　Nrp2 regulates OSN projection and MC migration in the MOB

(a) Targeting of OSN axons in the Nrp2 KOs.　Parasagittal MOB sections at P0 were analyzed by immunohistochemistry.　In the KOs, a coding sequence of the *Nrp2* has been deleted and replaced with that of *GFP*.　Thus, OSNs that are supposed to express Nrp2 can be detected with anti-GFP antibodies.　**(b)** MC migration in the Nrp2 KOs. Parasagittal sections at E18 were also analyzed by *in situ* hybridization using the *GFP* and *Nrp2* probes.　Dotted lines in the enlarged photos indicate the boundary of the GL and MCL.　n=7, 10, 6, 8 for the control, total KO, OSN-specific cKO, and MC-specific cKO, respectively.

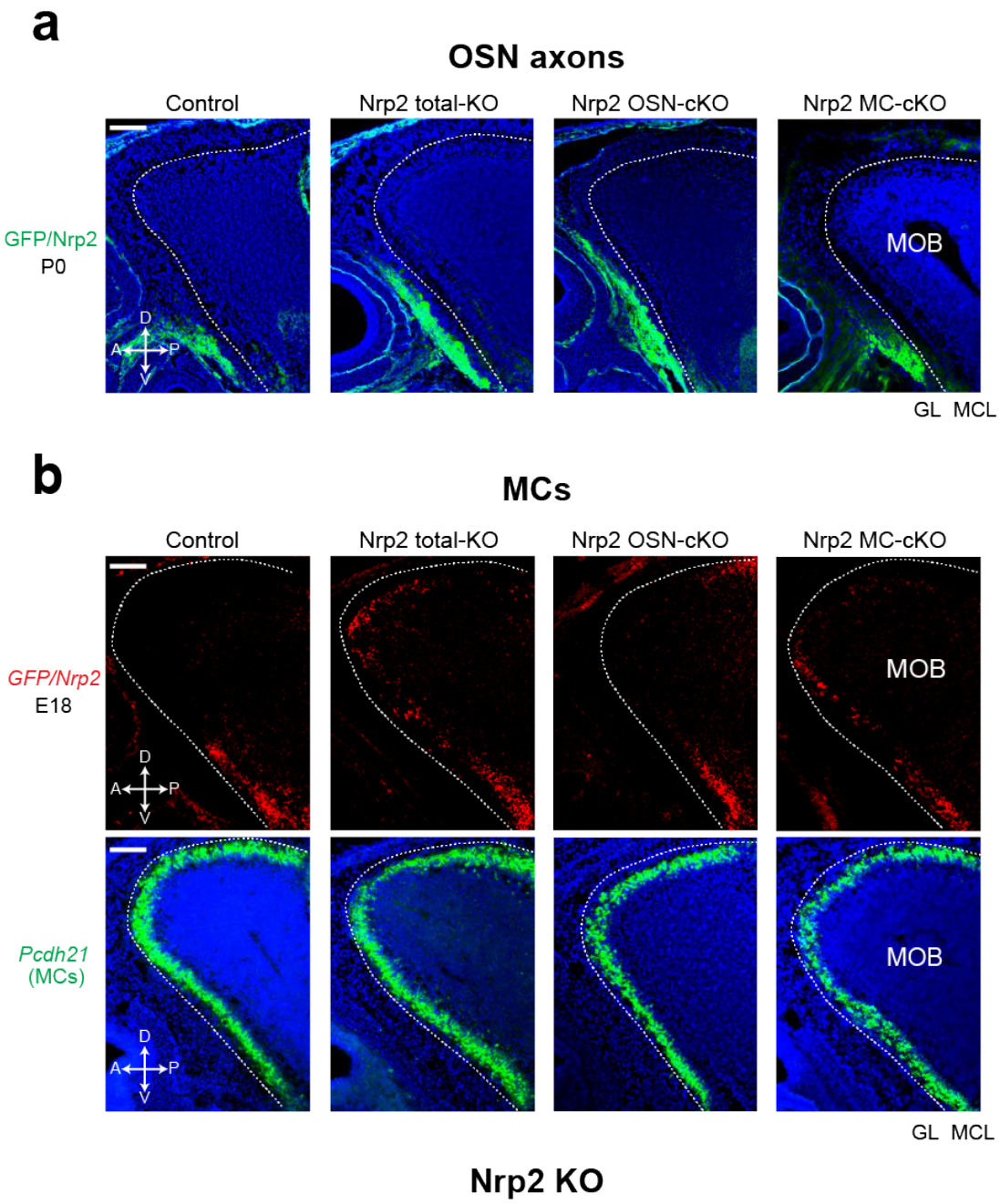
a
OSN axons
Control
Nrp2 total-KO
Nrp2 OSN-cKO
Nrp2 MC-cKO
GFP/Nrp2
P0
D
A
P
V
MOB
GL MCL
b
MCs
Control
Nrp2 total-KO
Nrp2 OSN-cKO
Nrp2 MC-cKO
GFP/Nrp2
E18
Pcdh21
(MCs)
MOB
GL MCL
Nrp2 KO

Fig. 11　Nrp2 regulates OSN projection and MC migration in the MOB

(a) Targeting of V-zone OSN axons in the Nrp2 KOs. To detect ventral OSN axons that normally express Nrp2, the *Nrp2* locus was replaced with the *GFP* in the KO allele. Parasagittal MOB sections at P0 were immunostained with anti-GFP antibodies. For the MC specific KO of Nrp2 (Nrp2 MC cKO), MOB sections were immunostained with anti-Nrp2 antibodies. **(b)** Distribution of *Nrp2*$^{+}$ MCs in the MOB in the Nrp2 KOs. Parasagittal sections at E18 were analyzed by *in situ* hybridization using probes for *GFP* and *Nrp2*, and *Pcdh21* (MC marker). Scale bars are 200 μm.

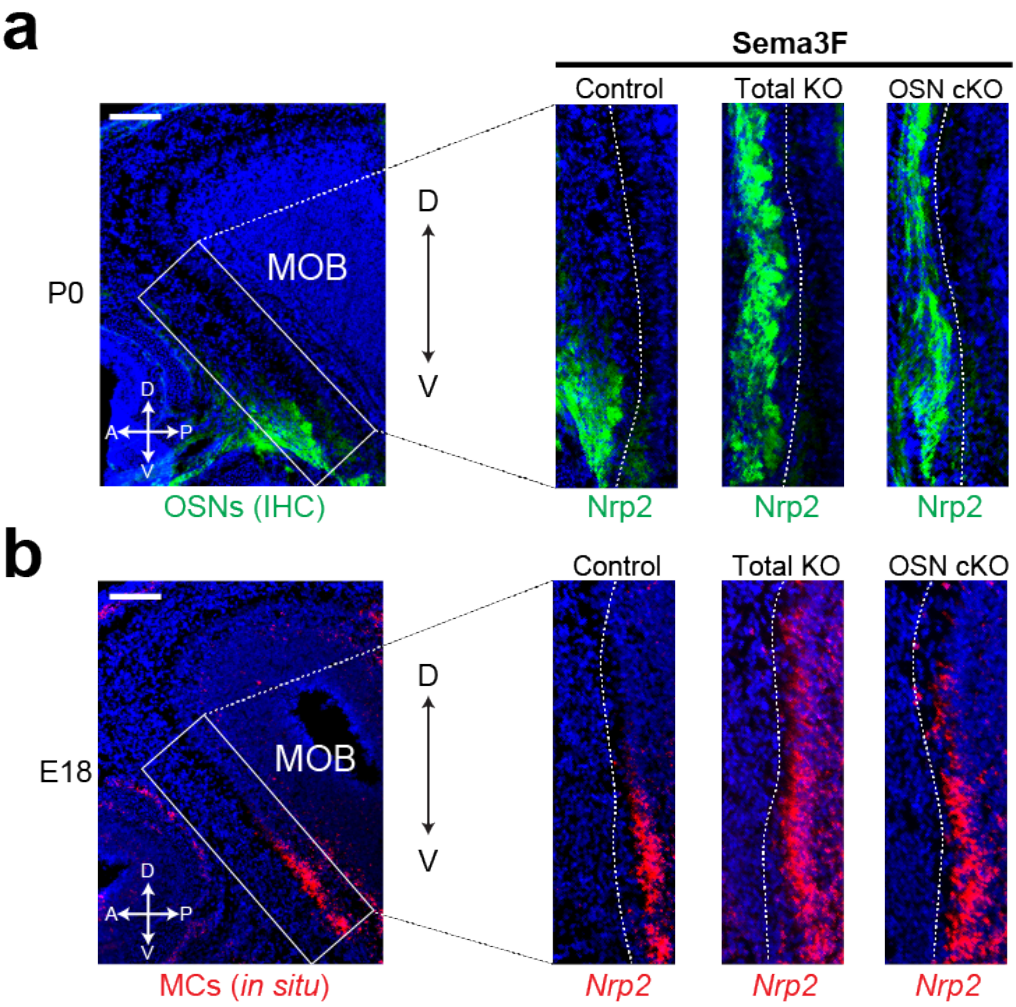
a
Sema3F
Control
Total KO
OSN cKO
P0
MOB
D
V
A
P
OSNs (IHC)
Nrp2
Nrp2
Nrp2
b
Control
Total KO
OSN cKO
E18
MOB
D
V
A
P
MCs (in situ)
Nrp2
Nrp2
Nrp2

Fig. 12 Sema3F co-regulates OSN projection and MC migration in the MOB.

(a) Targeting of OSN axons in the Sema3F KOs. Parasagittal MOB sections at P0 were immunostained with anti-Nrp2 antibodies. In the Sema3F total KO and OSN-specific Sema3F conditional KO (OSN cKO), $Nrp2^{+}$ OSNs are defasciculated and mistargeted to the dorsal MOB. Dotted lines in the enlarged photos indicate the boundary of the GL and MCL. (b) MC migration in the Sema3F KOs. Parasagittal MOB sections at E18 were also analyzed by *in situ* hybridization with the *Nrp2* probe (lower panel). n=7, 9, 6 for the control, total KO, and OSN-specific cKO, respectively. Scale bars are 200 μm. D, dorsal; V, ventral; A, anterior; P, posterior.

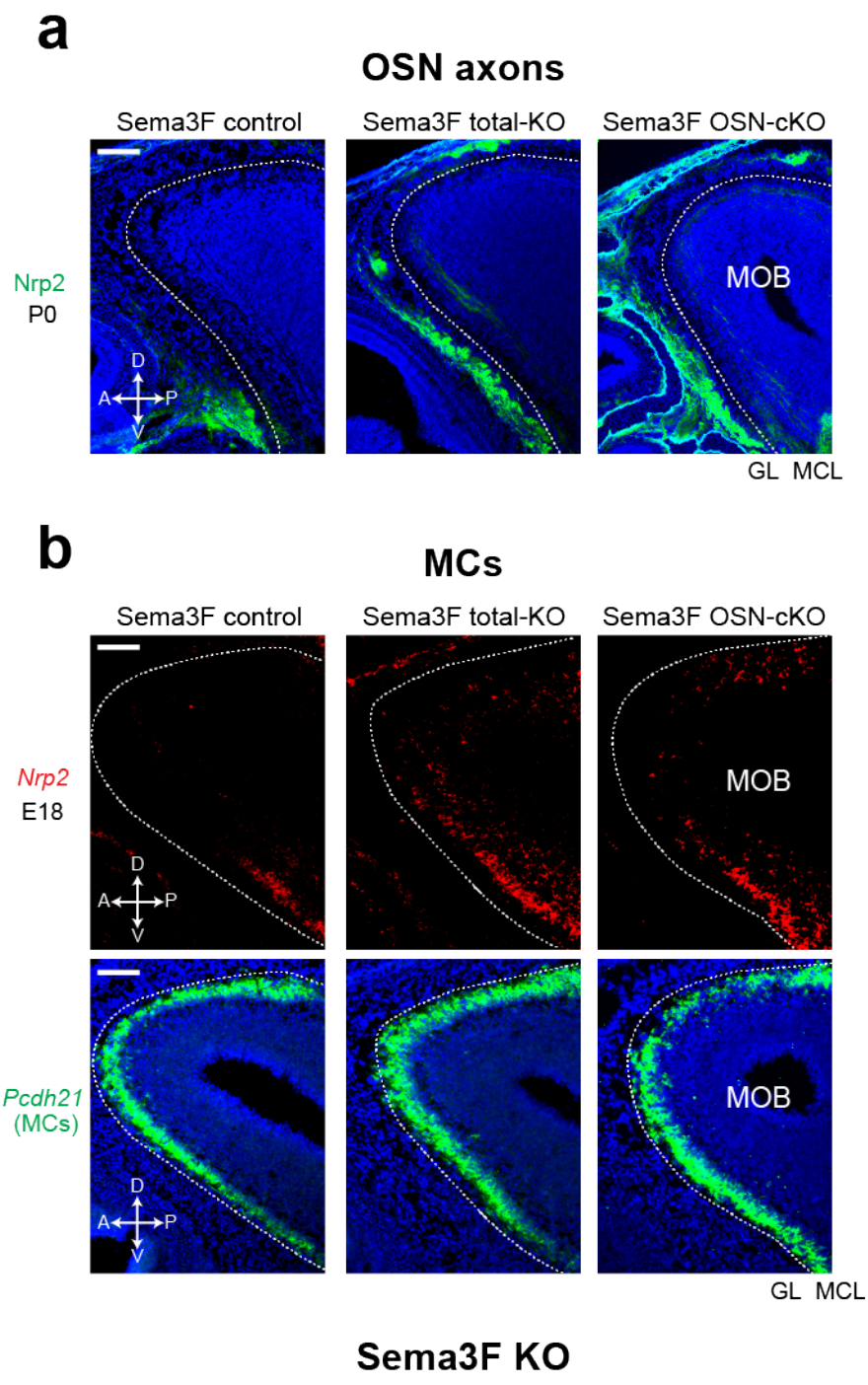
a
OSN axons
Sema3F control
Sema3F total-KO
Sema3F OSN-cKO
Nrp2
P0
D
A
P
V
MOB
GL MCL
b
MCs
Sema3F control
Sema3F total-KO
Sema3F OSN-cKO
Nrp2
E18
MOB
Pcdh21
(MCs)
MOB
GL MCL
Sema3F KO

Fig. 13 Nrp2-Sema3F repulsive interactions regulate both OSN projection and MC distribution in the MOB.

(a) Targeting of V-zone OSN axons in the Sema3F KOs. Parasagittal MOB sections at P0 were immunostained with anti-Nrp2 antibodies. **(b)** Distribution of *Nrp2*$^{+}$ MCs in the MOB in the Sema3F KOs. Parasagittal MOB sections at E18 were analyzed by *in situ* hybridization using probes for *Nrp2* and *Pcdh21* (MC marker). In all figures, broken lines indicate the boundary of the glomerular layer (GL) and mitral-cell layer (MCL) in the MOB. Scale bars are 200 μm.

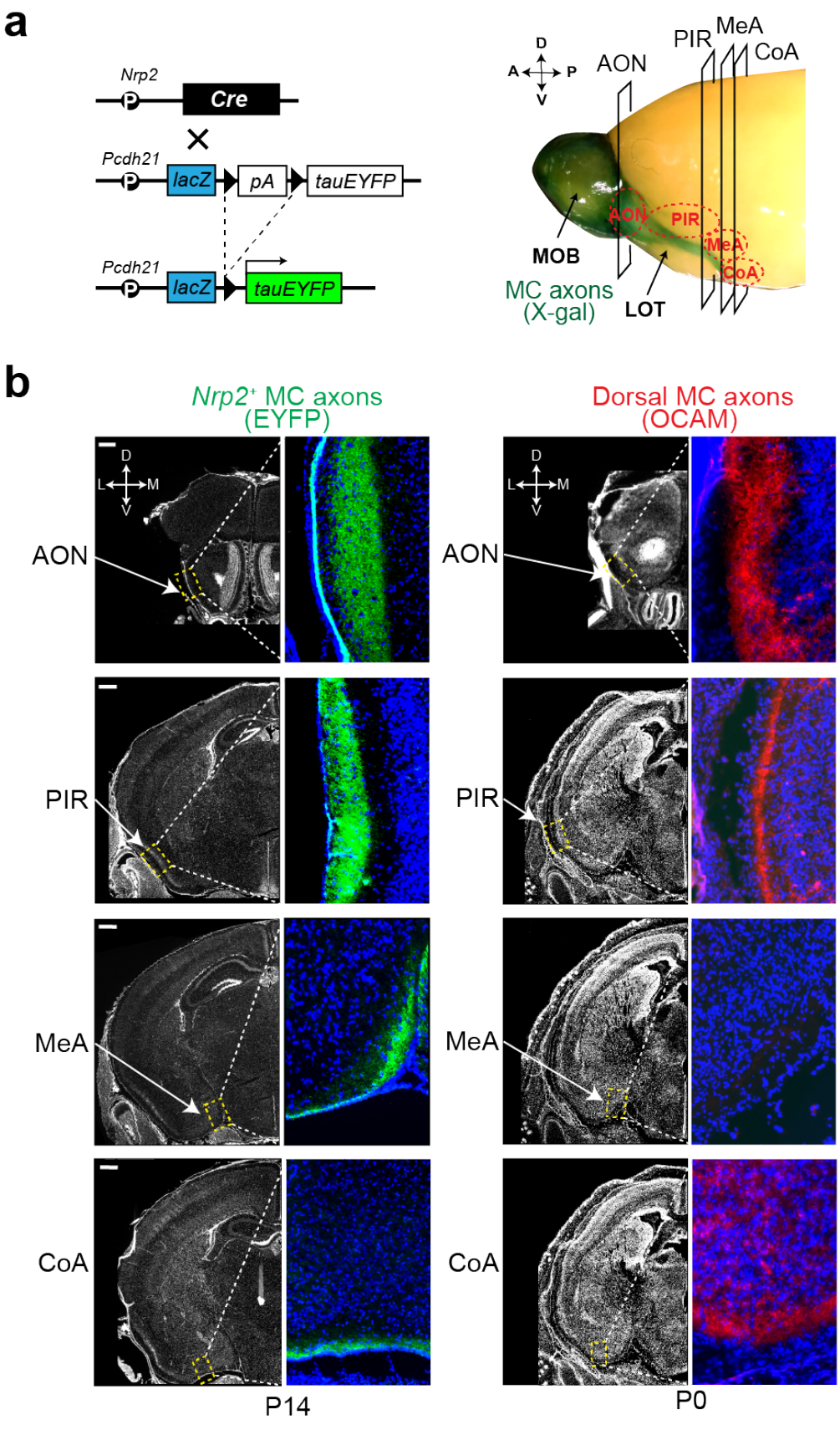
a
Nrp2
Cre
Pcdh21
lacZ
pA
tauEYFP
Pcdh21
lacZ
tauEYFP
D
A
P
V
AON
PIR
MeA
CoA
MOB
MC axons
(X-gal)
LOT
b
Nrp2+ MC axons
(EYFP)
Dorsal MC axons
(OCAM)
AON
PIR
MeA
CoA
P14
P0

Fig. 14 Axonal projection of Nrp2$^+$ MCs to the MeA.

(a) DNA constructs to detect the Nrp2$^+$ MC axons (left). The BAC Tg mouse Nrp2-Cre was crossed with another Tg mouse Pcdh21-lacZ-STOP-tauYFP. Since Nrp2 was difficult to detect in MOB MCs, Tg mice, in which the Nrp2-expressing MCs were labeled with EYFP, were generated. The *lacZ* was inserted into the construct to detect the promoter activity of *Pcdh21* by X-gal staining. Whole mount staining of the MOB is shown (right). Locations of coronal sections (AON, PIR, MeA) analyzed in (b) are indicated. **(b)** Detection of *Nrp2*$^+$ MC axons in the olfactory cortex (OC). Coronal sections of the OC at P14 were immunostained with anti-GFP antibodies to detect EYFP expressed in the *Nrp2*$^+$ MCs (left). *Nrp2*$^+$ ventral MC axons (green) project to the anterior olfactory nucleus (AON), piriform cortex (PIR), medial amygdala (MeA) and cortical amygdala (CoA). Coronal OC sections at P0 were immunostained with anti-OCAM antibodies (right). OCAM$^+$ dorsal MC axons (red) project to the AON and PIR, but not to the MeA. n=6. Scale bars are 100 μm. Nuclei are counterstained with DAPI in blue.

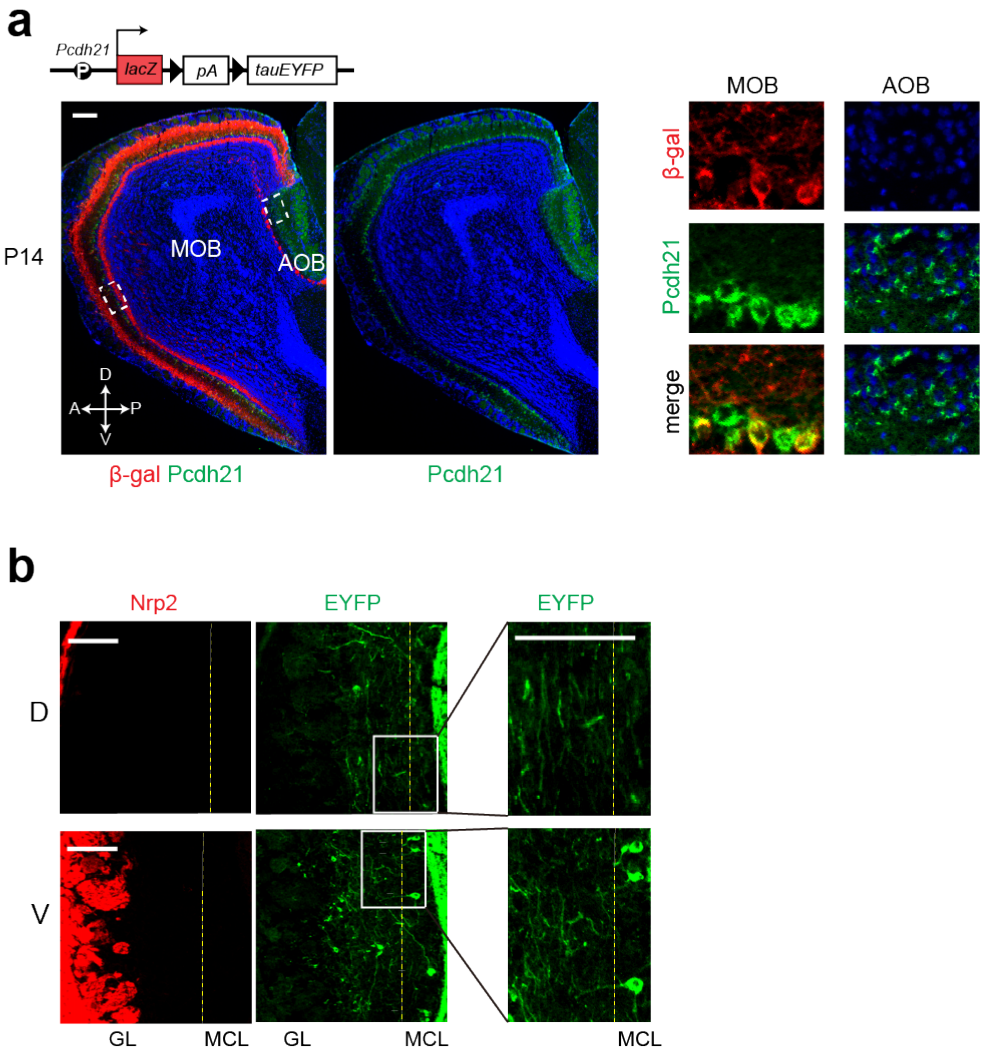
a
Pcdh21
lacZ
pA
tauEYFP
P14
MOB
AOB
D
A
P
V
β-gal Pcdh21
Pcdh21
MOB
AOB
β-gal
Pcdh21
merge
b
Nrp2
EYFP
EYFP
D
V
GL
MCL
GL
MCL
MCL

Fig. 15　Labeling of *Nrp2*$^{+}$ MCs in the MOB.

(a) MC-specific activation of the *Pcdh21* promoter in the MOB.　A parasagittal section at P14 was immunostained with antibodies against β-galactosidase (β-gal; red) and Pcdh21 (MC marker; green) (left).　Enlarged photos of the boxed regions are shown in the right.　Note that β-gal signals are detected in the MOB MCs, but not in the accessory olfactory bulb (AOB).　This mouse line is quite useful for the analysis of MOB MCs independent of AOB counterparts for axonal projection.　**(b)** V-region-specific activation of the *Nrp2* promoter in the MCL.　Nrp2-Cre mouse was crossed with the Tg mouse Pcdh21-lacZ-STOP-tauEYFP to induce EYFP specifically in the MOB MCs.　A coronal MOB section at P14 was immunostained with antibodies against GFP.　EYFP-positive MCs (green) are found in the ventral (V), but not in the dorsal (D) region of the MCL.　Scale bars are 100 μm.

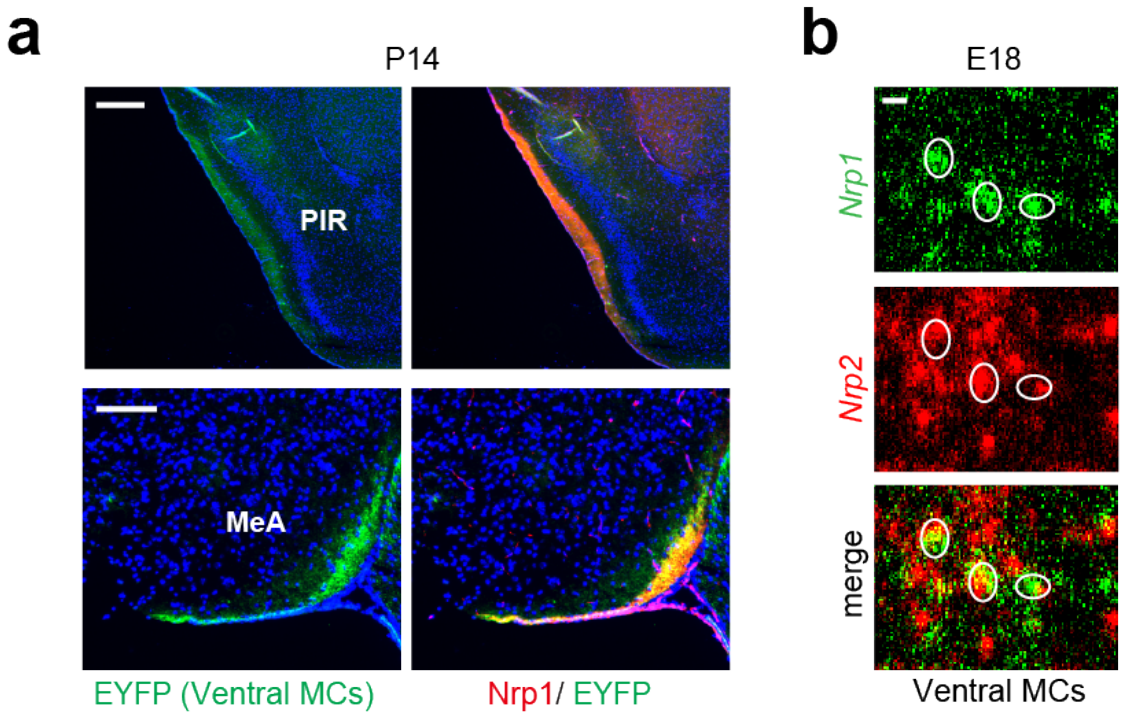

Fig. 16 ***Nrp2*$^{+}$ MCs of MOB also express *Nrp1*.**

(a) Detection of Nrp1 (MOB MC marker) in the *Nrp2*$^{+}$ (EYFP^{+}) ventral MC axons (green, left column). Coronal sections of the OC at P14 were immunostained with anti-GFP and anti-Nrp1 antibodies. GFP^{+} cells are all positive for Nrp1. **(b)** Double in situ hybridization of *Nrp1* and *Nrp2*. Scale bars are 100 μm in (a) and 10 μm in (b).

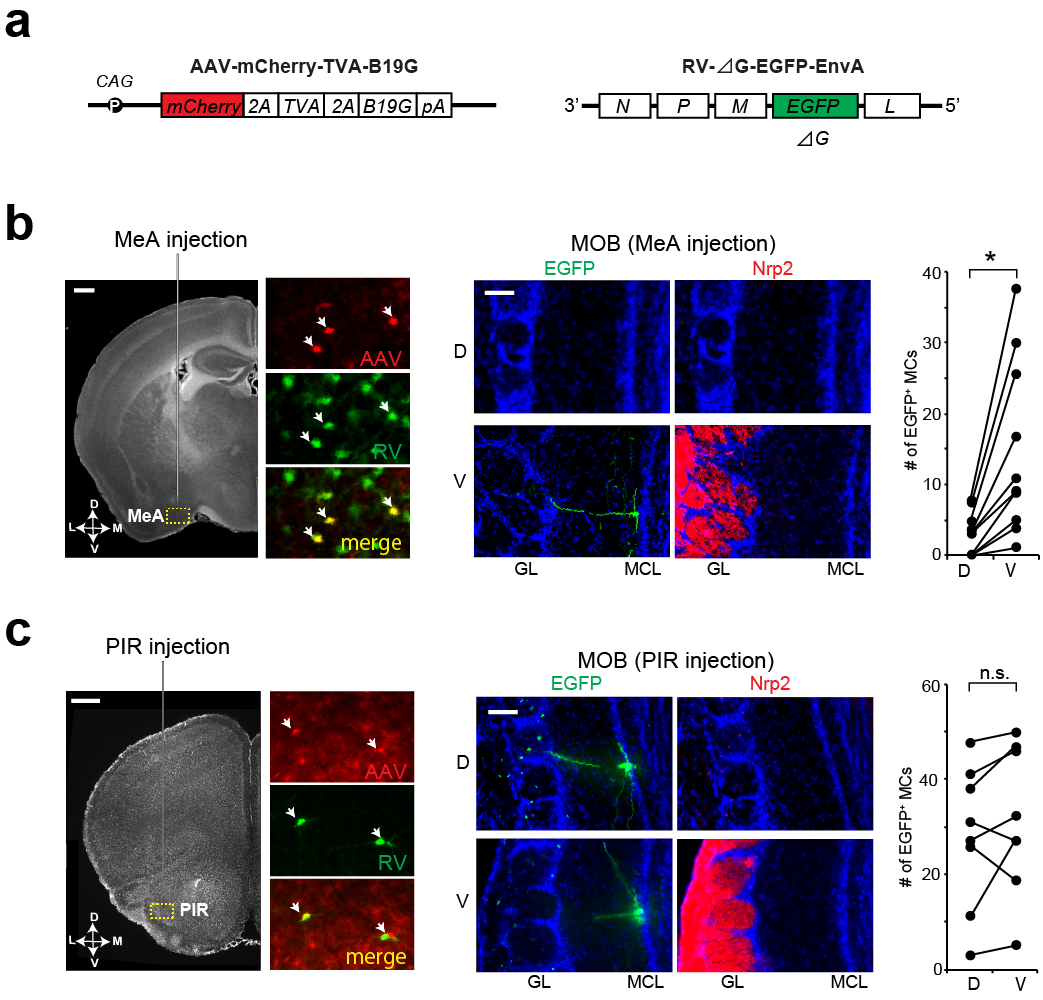
a
AAV-mCherry-TVA-B19G
CAG
mCherry
2A
TVA
2A
B19G
pA
RV-⊿G-EGFP-EnvA
3'
N
P
M
EGFP
L
5'
⊿G
b
MeA injection
MeA
AAV
RV
merge
MOB (MeA injection)
EGFP
Nrp2
D
V
GL
MCL
GL
MCL
*
# of EGFP+ MCs
40
30
20
10
0
D
V
c
PIR injection
PIR
AAV
RV
merge
MOB (PIR injection)
EGFP
Nrp2
D
V
GL
MCL
GL
MCL
n.s.
# of EGFP+ MCs
60
40
20
0
D
V

Fig. 17 Trans-synaptic tracing with the rabies virus.

(a) Virus constructs for circuit tracing. Structures of the adeno-associated virus (AAV) and rabies virus (RV) are schematically shown. In the RV construct, the *G* region has been deleted (Δ*G*) and replaced with *EGFP* [51]. **(b)** Virus injection into the MeA. AAV was first injected into the MeA region to complement TVA and glycoprotein G. After 2 weeks, the rabies virus was injected into the same MeA region to selectively infect neurons expressing the TVA receptor. After 10 days, serial coronal sections of the entire MeA were analyzed to determine whether the neurons infected with AAV and RV were indeed confined to the MeA. Double-labeled cells with mCherry for AAV and EGFP for RV are detected in the MeA. To detect the trans-synaptically labeled MCs, coronal sections of the MOB were immunostained with anti-GFP and anti-Nrp2 antibodies (right). EGFP-positive MCs are detected in the ventral (V), but not in the dorsal (D) region of the MOB. Numbers of EGFP-positive MCs in the dorsal (D) and ventral (V) MCs are compared in the right. Eighty-one starter MeA cells gave rise to 179 labeled MCs (n=10 mice). **P< 0.05 (Wilcoxon signed-rank test). **(c)** Virus injection to the PIR. Double-labeled cells with mCherry for AAV and EGFP for RV are detected in the PIR (left). To detect the trans-synaptically labeled MCs, coronal sections were immunostained with anti-GFP and anti-Nrp2 antibodies (right). EGFP-positive MCs are detected in both D and V regions of the MOB. Ninety-eight starter cells in the PIR resulted in 478 labeled MCs. n=8 mice. n.s.: not significant (Wilcoxon signed-rank test). Scale bars are 200 μm (left) and 100 μm (right).

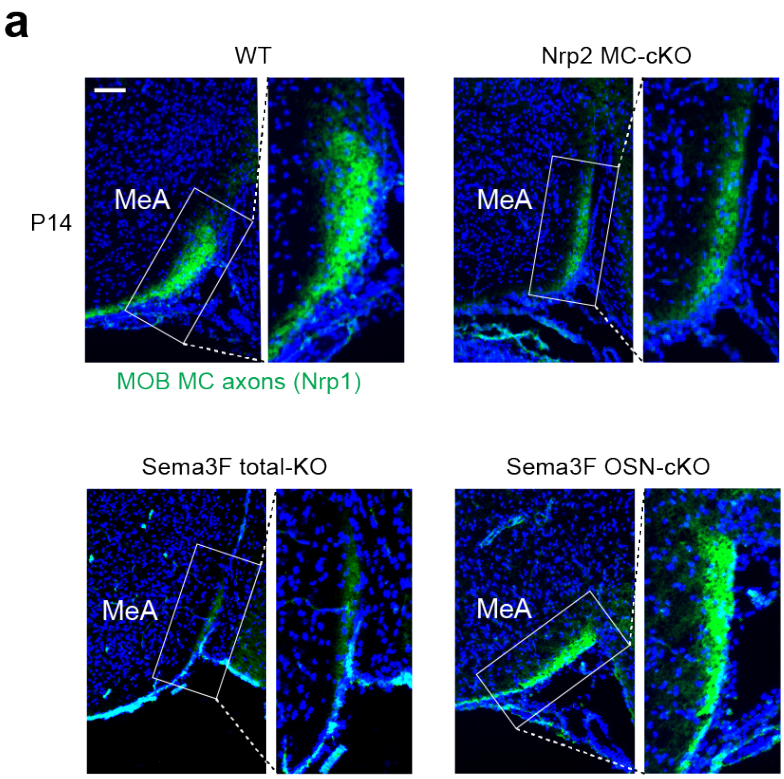
a
WT
Nrp2 MC-cKO
P14
MeA
MeA
MOB MC axons (Nrp1)
Sema3F total-KO
Sema3F OSN-cKO
MeA
MeA

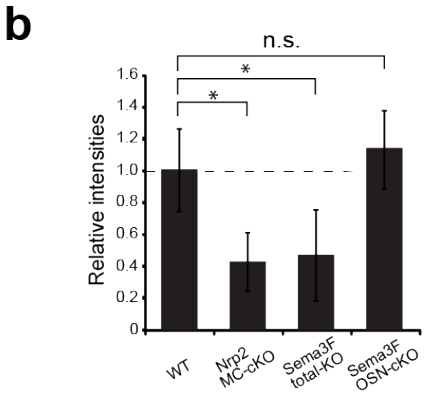
b
n.s.
*
*
Relative intensities
1.6
1.4
1.2
1.0
0.8
0.6
0.4
0.2
0
WT
Nrp2 MC-cKO
Sema3F total-KO
Sema3F OSN-cKO

Fig. 18　MC projection to the MeA is regulated by the Nrp2/Sema3F signaling.

(a) Detection of $Nrp2^+$ MC axons in the MeA.　MC axons projecting from the MOB at P14 are stained green with anti-Nrp1 antibodies.　Since Nrp2 signals in MOB MCs are hardly detected at this stage, anti-Nrp1 antibodies were used to detect MOB MC axons. Targeting of $Nrp1^+$ MC axons to the MeA is affected in the MC-specific cKO of Nrp2 and Sema3F total KO, but not in the OSN-specific Sema3F cKO (OSN cKO). **(b)** Nrp1-signals in the MeA.　Intensities of green staining ($Nrp1^+$) in the anterior MeA are compared between the WT and various KOs.　Nrp1 signals are reduced nearly by half in the MC-specific cKO of Nrp2 or Sema3F, but not in the OSN-specific cKO of Sema3F.　*P< 0.01, n.s.: not significant (Student's *t* test).

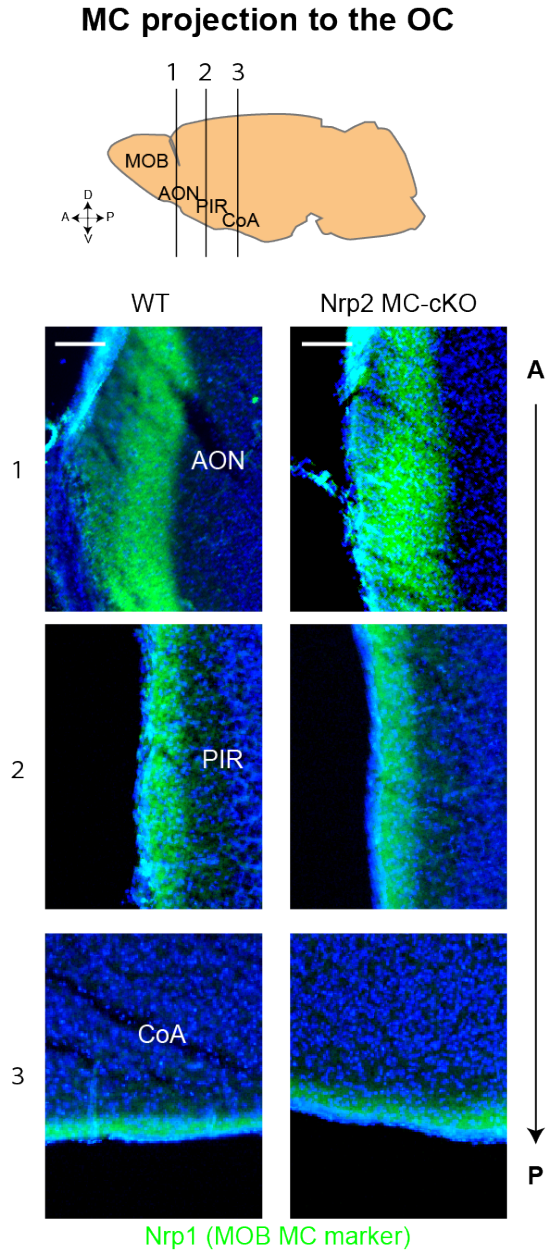

Fig. 19　Projection of MOB MCs to the OC.

Detection of MC axons in the OC. Coronal section of the OC at P14 were immunostained with antibodies against Nrp1 (MOB MC marker). Locations of OC sections are indicated at the top. Scale bars are 100 μm.

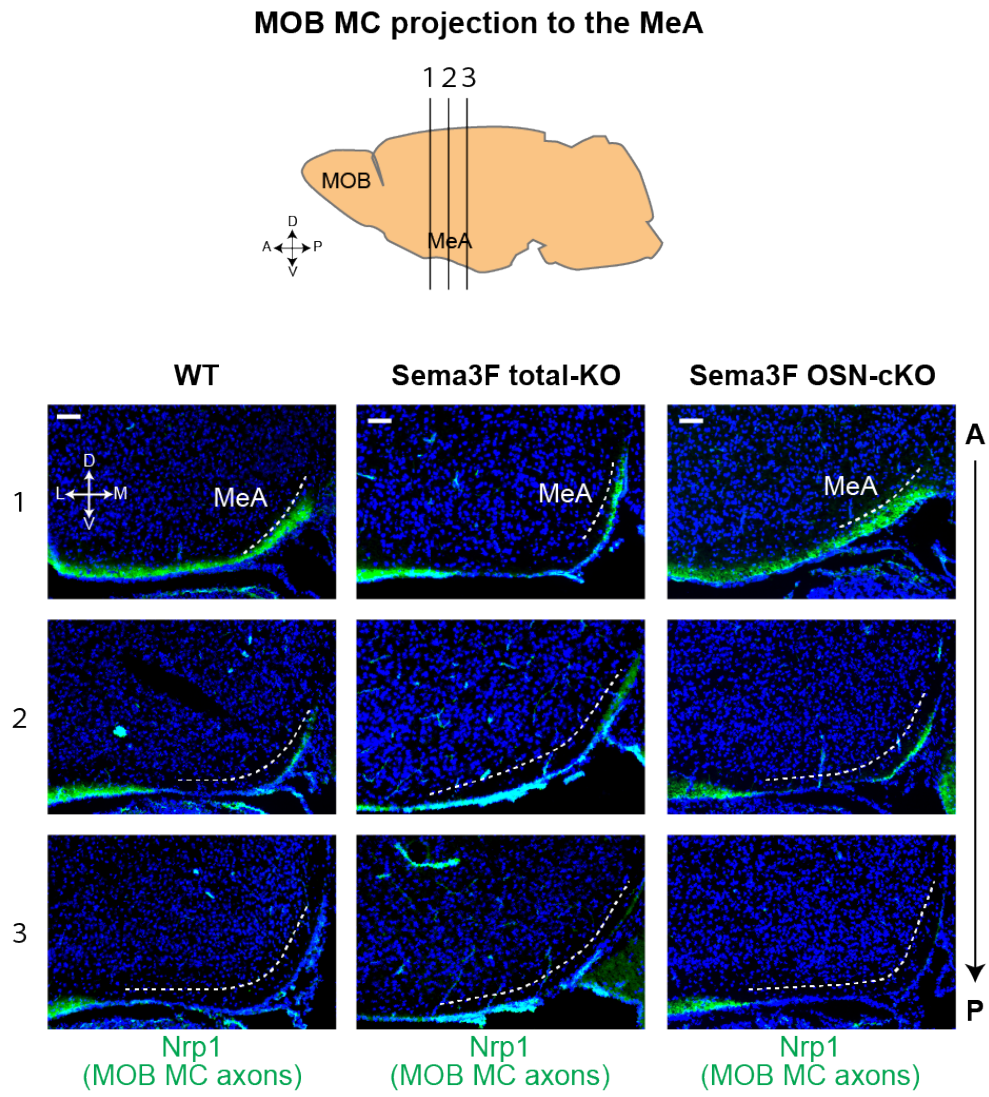

Fig. 20 MOB MC projection to the MeA in Sema3F KOs.

MOB MCs. Serial coronal sections (1~3) of the OC (each separated by 200 μm) at P14 were immunostained with antibodies against Nrp1 to detect MOB MC axons. $Nrp1^{+}$ axons (green) are defasciculated in the MeA region of the Sema3F total KO. As in the WT, Nrp1 signals are detected in the MeA in the OSN-specific Sema3F KO (OSN cKO). Scale bars are 100 μm.

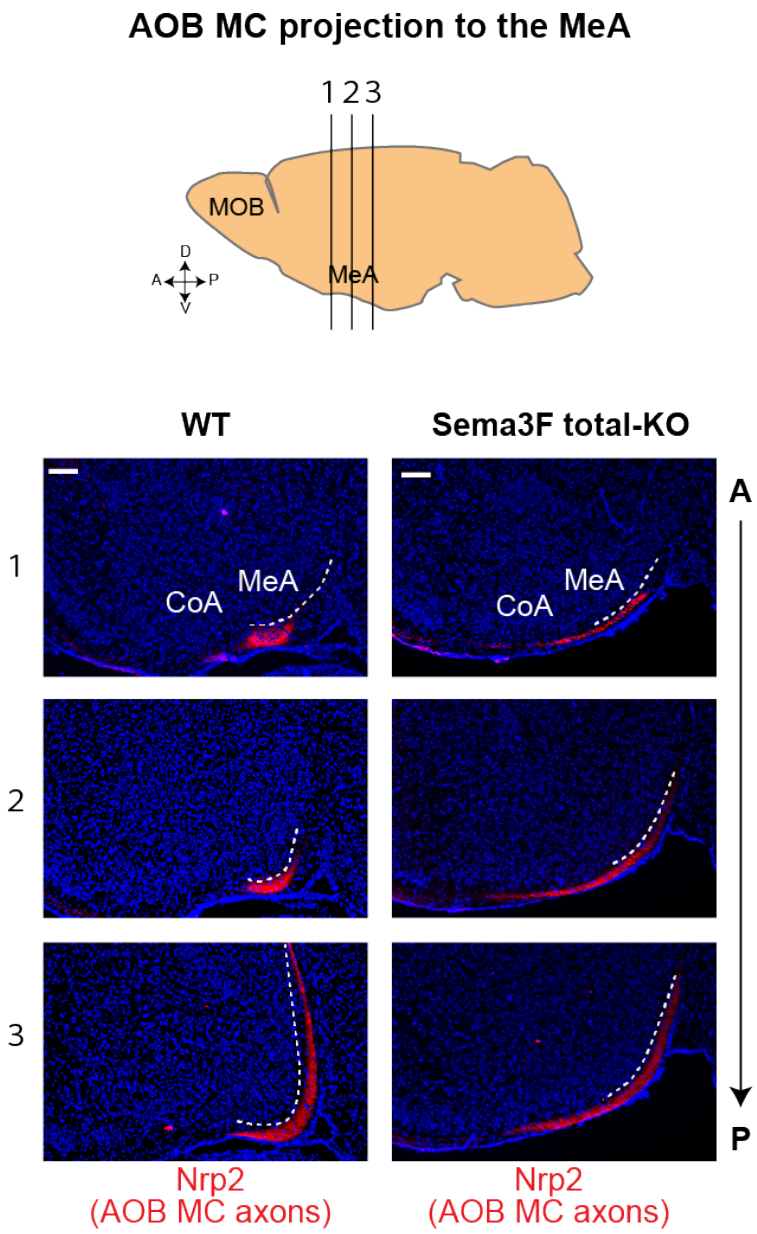

Fig. 21 AOB MC projection to the MeA

AOB MCs. Serial coronal sections (1~3) of the OC (each separated by 160 μm) at P14 were immunostained with antibodies against Nrp2 to detect AOB MC axons. Note that at this stage (P14), Nrp2 is not expressed in MOB MC axons. Thus, Nrp2 can be used as an AOB-MC marker. $Nrp2^{+}$ axons (red) are defasciculated in the MeA region of the Sema3F total KO. Broken lines in the sections indicate the MeA. Scale bars are 100 μm.

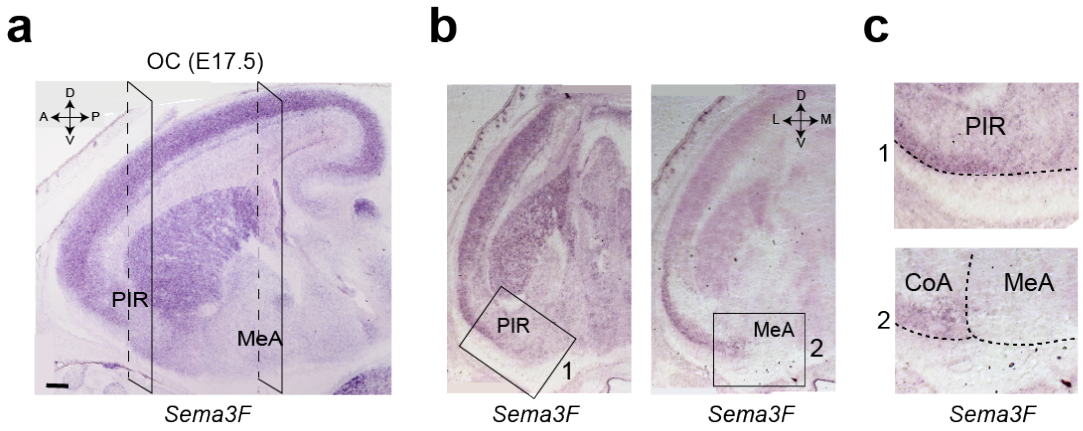

Fig. 22 *In situ* hybridization of *Sema3F* expression in the OC.

(a) A parasagittal section at E17.5 was hybridized with the *Sema3F* probes. **(b)** Coronal OC sections containing the PIR and MeA in (a) were analyzed. *Sema3F* transcripts are high in the PIR, but rarely detected in the MeA at the early embryonic stage. **(c)** Enlarged photos of PIR (1) and MeA (2) are shown in (b). Scale bar is 200 μm.

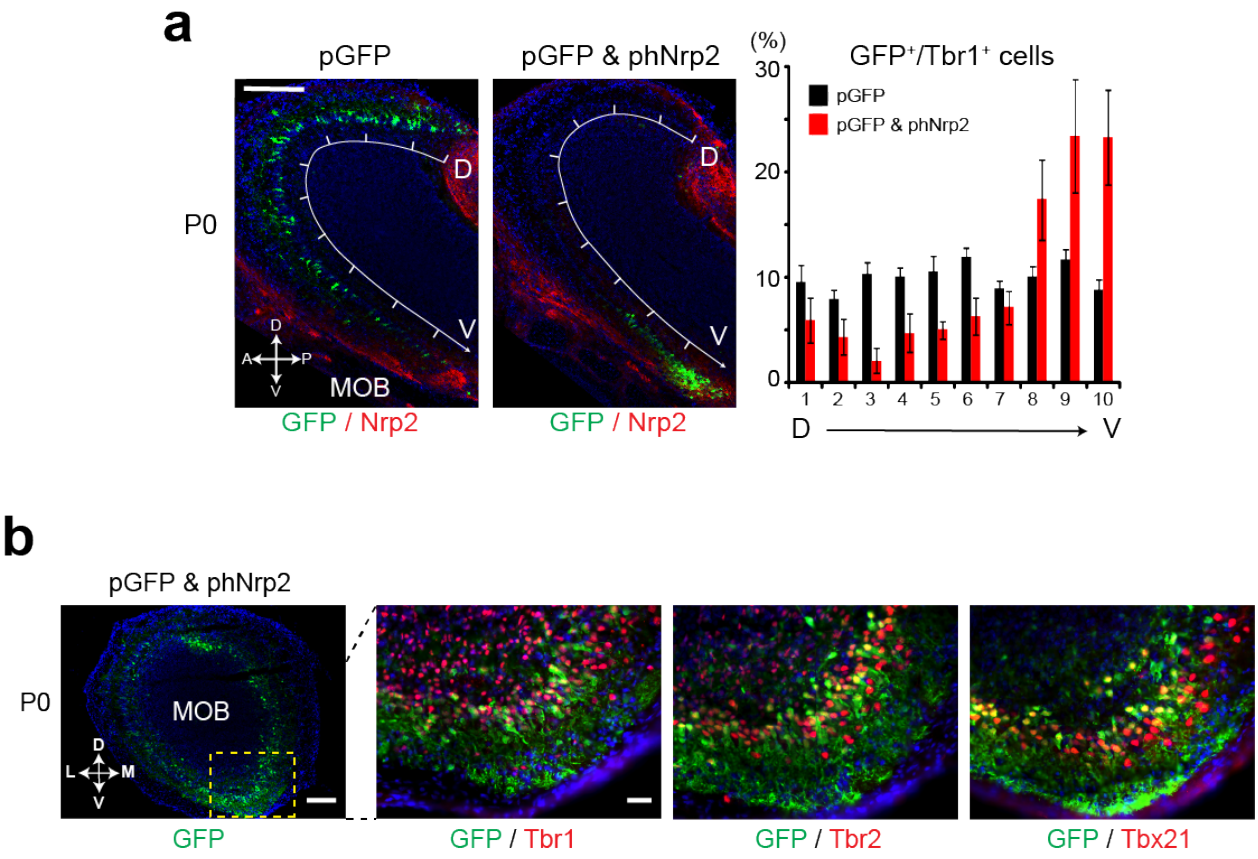

(From Dr. Imamura)

Fig. 23 *In utero* electroporation of the *Nrp2* Gene.

(a) *In Utero* electroporation of the embryonic MOB. Plasmid vectors containing *EGFP* cDNA (pGFP) with or without human *Nrp2* cDNA (phNrp2) were introduced into the MOB at E11. Parasagittal MOB sections at P0 were immunostained with antibodies against GFP (to detect ectopic $hNrp2^+$ MCs) and mouse Nrp2 (to detect endogenous $Nrp2^+$ MCs) (left). Note that the anti-mouse Nrp2 antibodies do not detect the human Nrp2. The MOB was dissected into ten sections along the D-V-axis and the distribution of GFP^+ $Tbr1^+$ MCs was analyzed. Statistical data are shown in the right. Ectopic expression of Nrp2 alone appears to direct migration of $EGFP^+$ MCs to the PV MOB. Data are presented in mean ±SE. **(b)** Plasmid vectors containing the *EGFP* (pGFP) with or without human *Nrp2* cDNA (phNrp2) were electroporated into the WT embryonic MOB at E11. Coronal MOB sections at P0 were isolated and immunostained with antibodies against GFP, Tbr1, Tbr2, and Tbx21 (MC markers). A fraction of MCs ectopically expressed EGFP. Scale bars are 200 μm in (a) 100 μm in (b left) and 20 μm in (b right).

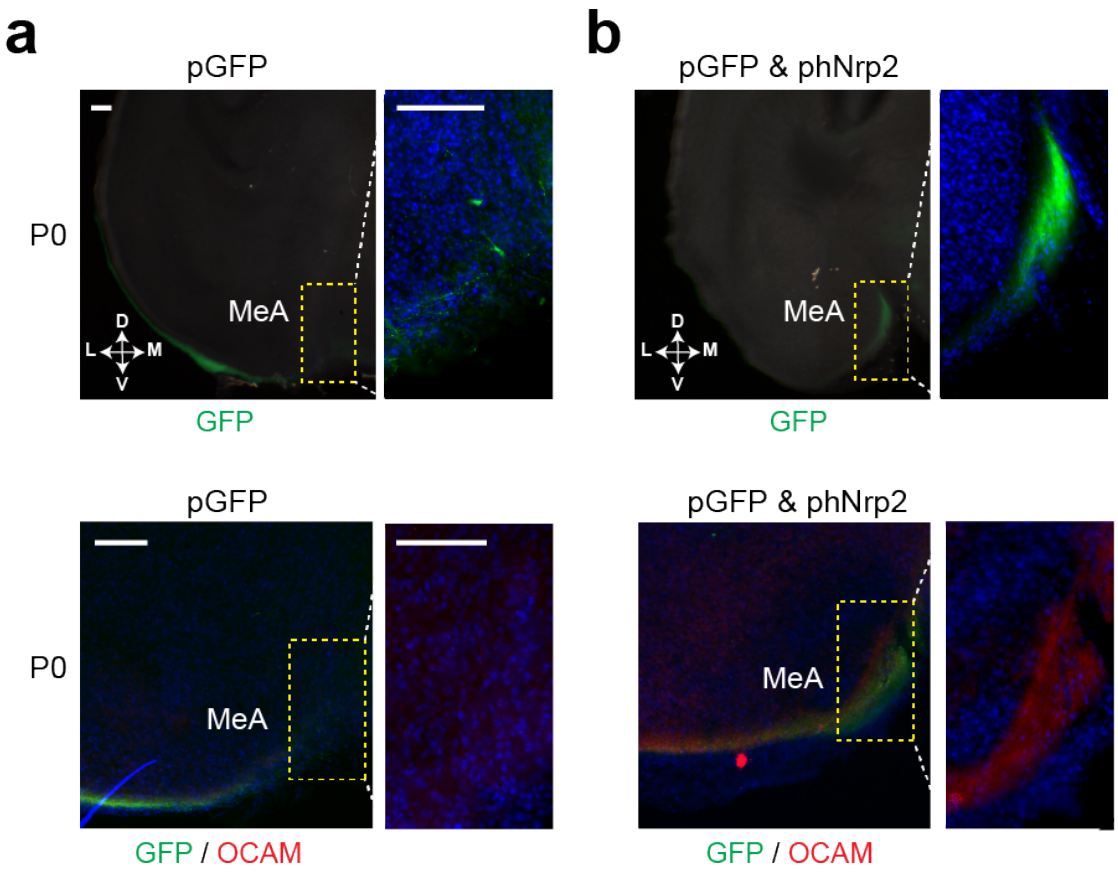

(From Dr. Imamura)

Fig. 24 Projection of electroporated hNrp2^{+} MCs to the MeA.

(a, b) *In Utero* electroporation of the embryonic MOB. Plasmid vectors containing *EGFP* cDNA (pGFP) with or without human *Nrp2* cDNA (phNrp2) were introduced into the MOB at E11. Coronal sections of the OC at P0 were immunostained with anti-GFP (green) and anti-OCAM antibodies (red). Note that the dorsal MC marker (OCAM) is detected with EGFP in the MeA, when the hNrp2 is ectopically expressed in MCs. Scale bars are 100 μm. Nuclei are counterstained with DAPI in blue.

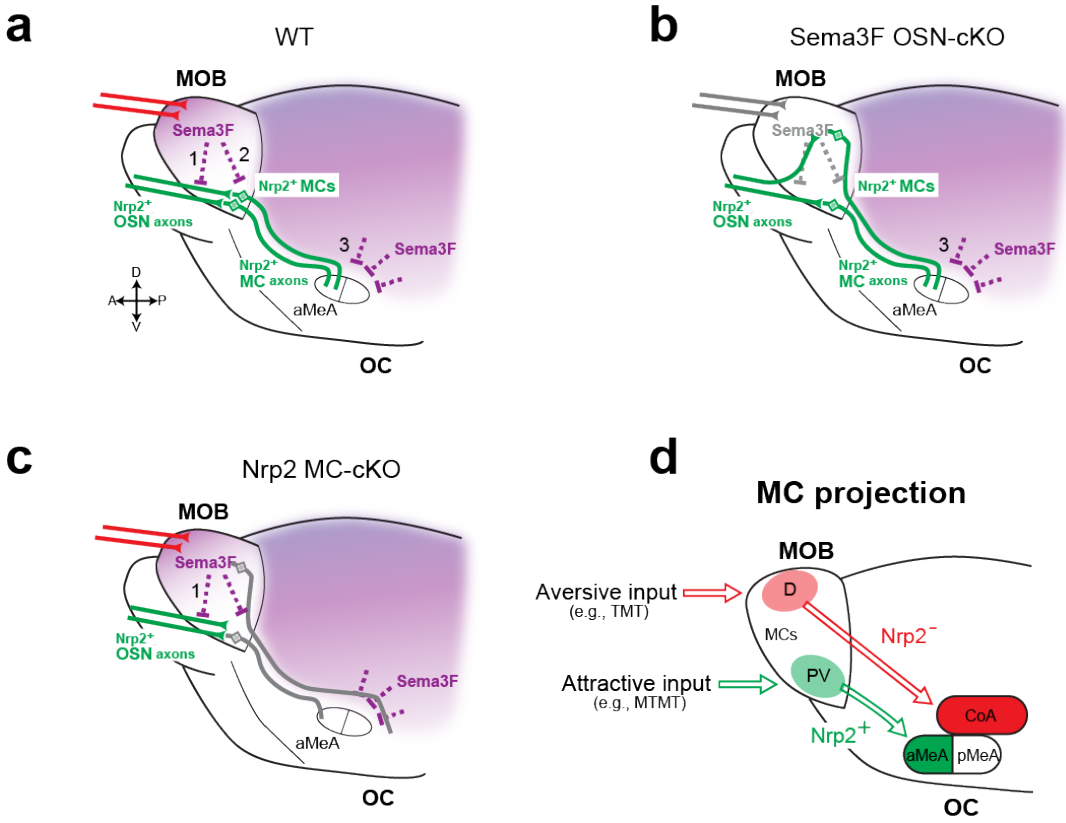
a
WT
MOB
Sema3F
1
2
Nrp2+ MCs
Nrp2+
OSN axons
3
Sema3F
Nrp2+
MC axons
aMeA
D
A
P
V
OC
b
Sema3F OSN-cKO
MOB
Sema3F
Nrp2+ MCs
Nrp2+
OSN axons
3
Sema3F
Nrp2+
MC axons
aMeA
OC
c
Nrp2 MC-cKO
MOB
Sema3F
1
Nrp2+
OSN axons
Sema3F
aMeA
OC
d
MC projection
MOB
Aversive input
(e.g., TMT)
D
MCs
Nrp2−
Attractive input
(e.g., MTMT)
PV
Nrp2+
CoA
aMeA
pMeA
OC

Fig. 25 Schematic diagrams of Nrp2$^+$ MC targeting.

(a) Sema3F-Nrp2 interactions in the olfactory circuit formation in the WT. A repulsive ligand, Sema3F, expressed by the dorsal-region OSNs is essential for guiding both Nrp2$^+$ OSN axons (1) and *Nrp2*$^+$ MCs to the ventral OB (2). OC-regions Sema3F instructs axon targeting of *Nrp2*$^+$ MCs to the MeA (3). **(b)** Targeting of Nrp2$^+$ MCs in the OSN-specific Sema3F cKO. Due to the absence of Sema3F in the dorsal MOB (1), distribution of Nrp2$^+$ MCs (2) is perturbed. However, targeting of Nrp2$^+$ MCs (3) to the anterior MeA (aMeA) is not affected. Nrp2$^+$ MCs remaining in the dorsal MOB in the cKO send their axons to the aMeA. **(c)** Targeting of MCs in the MC-specific Nrp2 cKO. Due to the absence of Nrp2 in MCs, both distribution (2) and targeting (3) of MCs are impaired in the cKO. MC axons from the MOB are significantly reduced in the aMeA. **(d)** A schematic diagram of the secondary projection in the mouse olfactory system. Aversive signals are reported to be transmitted from the dorsal MOB to the CoA. Nrp2$^+$ MCs convey the attractive social signals from the PV MOB to the anterior MeA (aMeA) but not to the posterior region (pMeA). Our present study revealed that activation of a single axon guidance gene, *Nrp2*, in MCs is sufficient to instruct olfactory circuit formation from the MOB to MeA.

5. Materials and methods

Mice

Tg Goofy-Cre (Kaneko-Goto et al., 2013) and Tg AP2ε-Cre (Feng et al., 2009) mice were obtained from Y. Yoshihara and T. Williams, respectively. The Nrp2-floxed, Sema3F-floxed, Rosa26-STOP-lacZ and Eno2-Cre mice were purchased from The Jackson Laboratory. Goofy-Cre, AP2ε-Cre, and Eno2-Cre mice were crossed with the Nrp2- or Sema3F-floxed mice to generate the OSN-specific, MC-specific, and total KO mice, respectively. To generate the *Nrp2-Cre* construct, the BAC clone RP24-250G22 containing the *Nrp2* promoter was modified and the *NiCre-pA-rpsL* sequence was introduced into the translation start site of *Nrp2*, using the Counter-Selection BAC Modification Kit (GENE BRIDGES). In the *Pcdh21* gene, an enhancer/promoter site was identified at ~10 kb upstream of the coding region (Nagai et al., 2005). The 10 kb fragment of *Pcdh21* was isolated from the BAC clone and introduced into the SKA vector. The *intron-tau-lacZ-STOP-ires-tauEYFP-pA* sequence was inserted into the *Pcdh21* minigene. Mice were housed in a 12-hr light/dark schedule and had free access to the food and water. Sample sizes were determined based on the standard procedure. No method was used to randomize the animals among the experimental group. The investigator was not blinded to the genotype, except for the pup suckling. Animal experiments were performed in accordance with the guideline of Animal Care Committees in the University of Tokyo, University of Fukui, Azabu University, and RIKEN Institute in Kobe.

Two-choice preference test

A custom-made acryl box (300 mm × 150 mm × 155 mm) was used, which contains three compartments; one mouse compartment (95 mm × 130 mm) and two sample compartments (190 mm × 65 mm). Urine was collected from 10 male and 10 female mice for 5 consecutive days. Each urine sample (60 μl) was applied to a piece of filter paper (40 mm×40 mm) and placed in a sample compartment in a counterbalanced manner between the tests. The partition between the mouse compartment and each sample compartment had a round vent that allowed air to pass and mice to poke their snouts through. A stream of air was drawn through a charcoal filter from each sample compartment to the mouse compartment with a vacuum pump. In the preference test, MC-specific Nrp2 cKO and littermate male (8-12 week-old) were analyzed. Each adult mouse was habituated for 5 min before the test. During subsequent 5-min, the amount of time that a mouse spent in poking its nose was measured (investigation time). The animal behavior was recorded with a digital video camera.

MTMT preference test

Castrated male urine was collected from 5 animals. Sexually experienced female mice were used to analyze the behavioral effects of MTMT in a urine preference test (Lin et al., 2005). A piece of filter paper spotted with 50 μl of castrated male urine alone or castrated male urine with 20 ppb MTMT was presented to the MC-specific Nrp2 cKO and littermate mice (8-12 week-old). Each adult mouse was habituated for 5 min prior to the test. In the subsequent 5-min duration, the amount of time spent for poking the nose was measured (investigation time). The animal behavior was recorded with a digital video camera.

Recording of ultrasonic vocalization

Ultrasonic sounds were detected using a condenser microphone (UltraSoundGate CM16/CMPA, Avisoft Bioacoustics). The microphone was connected to an A/D converter (UltraSoundGate 116; Avisoft Bioacoustics) with a sampling rate of 400 kHz, and acoustic signals were transmitted to a vocalization analysis system (SASLab Pro; Avisoft Bioacoustics) with frequency filters, a digital fast Fourier transform analyzer, and signal input-output terminals. In the test, Nrp2 MC-specific Nrp2 cKO and littermate male (8-12 week-old) were analyzed. n=10 for each genotype. Each adult male was habituated for 5 min prior to the test. The ultrasound was recorded for 6 min and the number of ultrasonic vocalizations was counted.

Viral injection

The mutant rabies virus (RV) ΔG-EGFP was obtained from Dr. Callaway, and amplified. RV-ΔG-EGFP-EnvA was produced as follows. BHK-EnvARGCD cells were plated in 12-well plates at 2E5 cells/well. The following day, the glycoprotein-deleted rabies virus SADDG-EGFP was added at an MOI of 1.5. The following day, the cells in each well were trypsinized and replated into a 10 cm plate. Virus-containing supernatants were harvested 2 days later, filter sterilized, and frozen at 80℃ in 1 ml aliquots (Wickersham et al., 2007). The AAV vector encoding TVA, Rabies glycoprotein and mCherry (pFBAAV-CAG-mCherry-TVA-B19G) was constructed from pAAV-EF1a-FLEX-GTB (a kind gift from Dr. Callaway), followed by viral packaging in Sf9 cells and purification as described (Kawashima et al., 2013). For trans-synaptic labeling, 0.5μl of AAV2/1-CAG-mCherry-TVA-B19G (2.0 x 10^{12} genome copy/ml) was injected into the brain at P60. During surgery, animals were

anesthetized with 400 mg/kg chloral hydrate and 44 mg/kg xylazine. For injection to the MeA, a needle was placed A/P -1.04 mm, M/L -1.9 mm from the bregma, D/V -5.4 mm from the surface. For injection to the PIR, a needle was placed A/P +1.5 mm, M/L -2.5 mm from the bregma, D/V -4.8 mm from the surface. After 2 weeks, RV-ΔG-EGFP-EnvA (10^7-10^8 plaque forming unit/ml) was injected into the same coordinate, MeA or PIR. Animals were then housed for 10 days to allow the virus to infect and spread trans-synaptically.

In utero electroporation

For *in utero electroporation* of the embryonic OB, pregnant mice were anesthetized by intraperitoneal injection of ketamine (100 mg/kg) and xylazine (10 mg/kg), and the uterine horns were taken out from the abdominal cavity (Imamura and Greer, 2015). Approximately 0.5 μl of DNA solution (1.5-4 μg/μl in 50% TE) was injected with a glass pipette into the lateral cerebral ventricle of embryos. To visualize the injection site, DNA solution was mixed with 100 μg/ml of Fast Green. Electroporation was carried out by applying square electric pulses. Two pulses of 30 V were given for 50 msec with a 950 msec interval. To efficiently label the MC precursors in the presumptive MOB, positive current was given from posterior to anterior. Following electroporation, the uterine horns were repositioned in the abdominal cavity, and animals were recovered in a warm environment after suturing.

Suckling behavior of pups

Lactating female mice were anesthetized and laid on the side exposing nipples toward pups. P0 pups were fasted for 4hr prior to the experiment, and placed 1 cm away from

the female's nipple. The time for finding nipples to suckle was measured within 4 min. Each pup was used only once in one stimulus condition. Experiments were performed in blind to the genotype of pups. The genotype was examined after each experiment.

Fear responses to TMT

Mice were habituated to a clean cage (23 x 16 x 12 cm) for 5 min before the test. A piece of filter paper spotted with 10 μl of undiluted TMT (Contech Enterprise Inc.) was presented to mice for 10 min. MC-specific Nrp2 cKO and littermate mice (8-12 week-old) were analyzed. n=10 for each genotype. The mouse behavior was recorded with a digital video camera. Average freezing time was measured.

Habituation-dishabituation test

A small perforated tube (1.5 ml microtube) with a piece of cotton spotted with 10 μl of 1% vanillin (or undiluted α-terpinene) was presented to the mouse for 1 min. This was repeated four times with 10-min intervals. In the fifth trial 10 min later, a 10 μl drop of undiluted α-terpinene (or 50 mM, 0.5 μM vanillin) was placed in the mouse cage. Habituation is defined by the progressive decrease of sniffing toward the repeated presentation of the same odor. Dishabituation is refined by the reinstatement of sniffing when the novel odor is presented. MC-specific cKO of Nrp2 and littermate mice (8-12 week-old) were analyzed. n=6 and 4 for each genotype in the 50 mM and 0.5 μM vanillin experiments, respectively.

In situ hybridization

Mice were perfused intracardially with 4% paraformaldehyde (PFA) in phosphate buffered saline (PBS). The brain samples were dissected and fixed overnight with 4% PFA in PBS. Parasagittal or coronal cryostat sections (10-20 μm each) were prepared from the frozen tissues in OCT compound (Tissue-Tek). To generate RNA probes for in situ hybridization, DNA fragments of 500-1000 bp were amplified by PCR from cDNA of the mouse brain (C57BL/6). Only unique sequences were amplified for each probe. PCR products were subcloned into pGEM-T (Promega) and used as templates to make probes. Digoxigenin (DIG)-labeled probes were prepared with the DIG RNA labeling kit (Roche). For in situ hybridization, samples were fixed in 4% paraformaldehyde in PBS for 15 min at 4°C (Takeuchi et al., 2010; Tsuboi et al., 1999). The sections were rinsed with PBS and incubated with 7 μg/ml Proteinase K in 10 mM Tris-Cl, pH 7.4, 1 mM EDTA for 10min at 37°C. After fixing again with 4% paraformaldehyde in PBS for 10min, the sections were incubated with 0.25% acetic anhydride and 0.1 M triethanolamine, pH 8.0, washed with PBS, and air-dried. Sections were incubated for 16hr at 51°C with probes in the hybridization buffer. After incubation, the sections were washed, first with 2×SSC-50% formamide, then with 2×SSC, and finally with 0.2×SSC twice for 20 min at 65°C. After blocking with the blocking reagent (Roche), slides were incubated with the alkaline phosphatase (AP)-conjugated anti-DIG antibody (Roche). Probe-positive cells were stained purple with nitroblue tetrazolium salt (NBT) and 5-bromo-4-chloro-3-indolyl phosphate toludinium salt (BCIP). For fluorescence in situ hybridization, probe-positive cells were stained with a HNPP/FastRed (Roche) in the staining buffer (100 mM Tris-Cl pH 8.0, 100 mM NaCl, 5 mM $MgCl_2$). After washing with PBS three times, samples were

photographed with a confocal microscope, model BX61 (Olympus). Boundaries of brain structures were determined according to the standard atlas (Franklin and Paxinos, 2008; Schambra et al.).

Immunohistochemistry

Immunohistochemistry was performed according to the published procedure (Serizawa et al., 2006) using the following antibodies: anti-Nrp1 (1:500; R&D systems), anti-Nrp2 (1:500; R&D systems), anti-GFP (1:1000; Clontech), anti-β-galactosidase (1:1000; ICN biochemicals), anti-OCAM (1:500; R&D systems), rabbit anti-Tbr1 (1:5000; Abcam), rabbit anti-Tbr2 (1:5000; Abcam), anti-BrdU (1:200; Abcam), and rabbit anti-Tbx21 (1:10,000; provided by Dr. Yoshihara at RIKEN). Antibodies against Pcdh-21 were generated by immunizing guinea pigs with KLH-conjugated synthetic peptides as described previously (Takeuchi et al., 2010). Alexa fluor conjugated secondary antibodies (Invitrogen) were used at 1:200 dilution.

X-gal Staining

Animals were perfused intracardially with 4% paraformaldehyde in PBS and olfactory tissue sections were prepared. The sections were washed with PBS three times and treated with X-gal staining buffer (5 mM potassium ferricyanide, 5 mM potassium ferrocyanide, 2 mM $MgCl_2$, 0.01% sodium deoxycholate, 0.02% Nonidet P-40 (NP-40), 1 mg/ml X-gal in PBS) with gentle agitation. The blue precipitate was generated by incubating overnight at 37°C in the dark. The sections were photographed with an Olympus Optical AX70 microscope (Olympus).

BrdU labeling

Labeling of 5-bromodeozyuridine (BrdU) was performed as described previously (Biffo et al., 1992). BrdU was intraperitoneally injected into the pregnant mice (100 mg/kg) at pregnant day 9, 10, 11, 12, 13 and 14. OB sections were prepared from the E18.5 embryo, and washed three times with PBS at room temperature for 5 min, incubated in 1.2 N HCl at 37°C for 1 hour, rinsed in 100 mM borate buffer (pH 8.5) at room temperature for 1 min twice, and in PBS briefly. Then, the BrdU was stained with anti-BrdU antibodies.

Plasmids

A plasmid vector containing the *egfp* cDNA with CAG enhancer (pGFP) was obtained from Addgene (pCAG-GFP; Plasmid #11150). To construct pNrp2, full-length human nrp2 cDNA was cloned with PCR using the template plasmid (Clone; HsCD00443185) from DNASU. Primer sequences used were: AGTGATATCCACCATGGATATGTTTCCTCTCACC; and AGTGATATCTCATGCCTCGGAGCAGCACTTTTGG. The obtained PCR fragment was inserted into the pCAGEN vector (Addgene; Plasmid #11160).

Intensity measurements and statistical analyses

Optical Images were photographed with an Olympus Optical AX70 microscope. Fluorescent images were photographed with a fluorescence microscope, Olympus model IX70 equipped with a cooled CCD camera, C4742-95-12ERG (Hamamatsu Photonics). For quantification, the tone was reversed and monochrome images were

used. Staining intensities were measured with ImageJ. All statistical analyses were performed with Excel 2010 (Microsoft).

6. References

Biffo, S., Verdun di Cantogno, L., and Fasolo, A. (1992). Double labeling with non-isotopic in situ hybridization and BrdU immunohistochemistry: calmodulin (CaM) mRNA expression in post-mitotic neurons of the olfactory system. J Histochem Cytochem *40*, 535-540.

Blanchart, A., De Carlos, J.A., and Lopez-Mascaraque, L. (2006). Time frame of mitral cell development in the mice olfactory bulb. J Comp Neurol *496*, 529-543.

Buck, L., and Axel, R. (1991). A novel multigene family may encode odorant receptors: a molecular basis for odor recognition. Cell *65*, 175-187.

Choi, G.B., Dong, H.W., Murphy, A.J., Valenzuela, D.M., Yancopoulos, G.D., Swanson, L.W., and Anderson, D.J. (2005). Lhx6 delineates a pathway mediating innate reproductive behaviors from the amygdala to the hypothalamus. Neuron *46*, 647-660.

de Olmos, J., Hardy, H., and Heimer, L. (1978). The afferent connections of the main and the accessory olfactory bulb formations in the rat: an experimental HRP-study. J Comp Neurol *181*, 213-244.

Devor, M. (1976). Fiber trajectories of olfactory bulb efferents in the hamster. J Comp Neurol *166*, 31-47.

DiBenedictis, B.T., Ingraham, K.L., Baum, M.J., and Cherry, J.A. (2012). Disruption of urinary odor preference and lordosis behavior in female mice given lesions of the medial amygdala. Physiol Behav *105*, 554-559.

Doty, R.L. (1986). Odor-guided behavior in mammals. Experientia *42*, 257-271.

Duan, X., Block, E., Li, Z., Connelly, T., Zhang, J., Huang, Z., Su, X., Pan, Y., Wu, L., Chi, Q.*, et al.* (2012). Crucial role of copper in detection of metal-coordinating odorants. Proc Natl Acad Sci U S A *109*, 3492-3497.

Dulac, C., and Torello, A.T. (2003). Molecular detection of pheromone signals in mammals: from genes to behaviour. Nat Rev Neurosci *4*, 551-562.

Feng, W., Simoes-de-Souza, F., Finger, T.E., Restrepo, D., and Williams, T. (2009). Disorganized olfactory bulb lamination in mice deficient for transcription factor AP-2epsilon. Mol Cell Neurosci *42*, 161-171.

Feng, W., and Williams, T. (2003). Cloning and characterization of the mouse AP-2 epsilon gene: a novel family member expressed in the developing olfactory bulb. Mol Cell Neurosci *24*, 460-475.

Franklin, K., and Paxinos, G. (2008). The Mouse Brain in Stereotaxic Coordinates, third edn (Academic press).

Garrosa, M., Gayoso, M.J., and Esteban, F.J. (1998). Prenatal development of the mammalian vomeronasal organ. Microsc Res Tech *41*, 456-470.

Ghosh, S., Larson, S.D., Hefzi, H., Marnoy, Z., Cutforth, T., Dokka, K., and Baldwin, K.K. (2011). Sensory maps in the olfactory cortex defined by long-range viral tracing of single neurons. Nature *472*, 217-220.

Giger, R.J., Urquhart, E.R., Gillespie, S.K., Levengood, D.V., Ginty, D.D., and Kolodkin, A.L. (1998). Neuropilin-2 is a receptor for semaphorin IV: insight into the structural basis of receptor function and specificity. Neuron *21*, 1079-1092.

Hinds, J.W. (1968). Autoradiographic study of histogenesis in the mouse olfactory bulb. I. Time of origin of neurons and neuroglia. J Comp Neurol *134*, 287-304.

Hirata, T., and Fujisawa, H. (1999). Environmental control of collateral branching and target invasion of mitral cell axons during development. J Neurobiol *38*, 93-104.

Hong, W., Kim, D.W., and Anderson, D.J. (2014). Antagonistic control of social versus repetitive self-grooming behaviors by separable amygdala neuronal subsets. Cell *158*, 1348-1361.

Hudson, R., and Distel, H. (1986). Pheromonal release of suckling in rabbits does not depend on the vomeronasal organ. Physiol Behav *37*, 123-128.

Imai, T., Yamazaki, T., Kobayakawa, R., Kobayakawa, K., Abe, T., Suzuki, M., and Sakano, H. (2009). Pre-target axon sorting establishes the neural map topography. Science *325*, 585-590.

Imamura, F., and Greer, C.A. (2015). Segregated labeling of olfactory bulb projection neurons based on their birthdates. Eur J Neurosci *41*, 147-156.

Inaki, K., Nishimura, S., Nakashiba, T., Itohara, S., and Yoshihara, Y. (2004). Laminar organization of the developing lateral olfactory tract revealed by differential expression of cell recognition molecules. J Comp Neurol *479*, 243-256.

Kaneko-Goto, T., Sato, Y., Katada, S., Kinameri, E., Yoshihara, S., Nishiyori, A., Kimura, M., Fujita, H., Touhara, K., Reed, R.R.*, et al.* (2013). Goofy coordinates the acuity of olfactory signaling. J Neurosci *33*, 12987-12996, 12996a.

Kang, N., Baum, M.J., and Cherry, J.A. (2009). A direct main olfactory bulb projection to the 'vomeronasal' amygdala in female mice selectively responds to volatile pheromones from males. Eur J Neurosci *29*, 624-634.

Kawashima, T., Kitamura, K., Suzuki, K., Nonaka, M., Kamijo, S., Takemoto-Kimura, S., Kano, M., Okuno, H., Ohki, K., and Bito, H. (2013). Functional labeling of neurons and their projections using the synthetic activity-dependent promoter E-SARE. Nat Methods *10*, 889-895.

Keller, M., Douhard, Q., Baum, M.J., and Bakker, J. (2006). Destruction of the main olfactory epithelium reduces female sexual behavior and olfactory investigation in female mice. Chem Senses *31*, 315-323.

Kimchi, T., Xu, J., and Dulac, C. (2007). A functional circuit underlying male sexual behaviour in the female mouse brain. Nature *448*, 1009-1014.

Kobayakawa, K., Kobayakawa, R., Matsumoto, H., Oka, Y., Imai, T., Ikawa, M., Okabe, M., Ikeda, T., Itohara, S., Kikusui, T.*, et al.* (2007). Innate versus learned odour processing in the mouse olfactory bulb. Nature *450*, 503-508.

Kolodkin, A.L., Levengood, D.V., Rowe, E.G., Tai, Y.T., Giger, R.J., and Ginty, D.D.

(1997). Neuropilin is a semaphorin III receptor. Cell *90*, 753-762.

Lehman, M.N., Winans, S.S., and Powers, J.B. (1980). Medial nucleus of the amygdala mediates chemosensory control of male hamster sexual behavior. Science *210*, 557-560.

Leypold, B.G., Yu, C.R., Leinders-Zufall, T., Kim, M.M., Zufall, F., and Axel, R. (2002). Altered sexual and social behaviors in trp2 mutant mice. Proc Natl Acad Sci U S A *99*, 6376-6381.

Lin, D.Y., Zhang, S.Z., Block, E., and Katz, L.C. (2005). Encoding social signals in the mouse main olfactory bulb. Nature *434*, 470-477.

Mandiyan, V.S., Coats, J.K., and Shah, N.M. (2005). Deficits in sexual and aggressive behaviors in Cnga2 mutant mice. Nat Neurosci *8*, 1660-1662.

Maras, P.M., and Petrulis, A. (2006). Chemosensory and steroid-responsive regions of the medial amygdala regulate distinct aspects of opposite-sex odor preference in male Syrian hamsters. Eur J Neurosci *24*, 3541-3552.

Martel, K.L., and Baum, M.J. (2007). Sexually dimorphic activation of the accessory, but not the main, olfactory bulb in mice by urinary volatiles. Eur J Neurosci *26*, 463-475.

McBride, K., and Slotnick, B. (2006). Discrimination between the enantiomers of carvone and of terpinen-4-ol odorants in normal rats and those with lesions of the olfactory bulbs. J Neurosci *26*, 9892-9901.

Meisami, E., and Bhatnagar, K.P. (1998). Structure and diversity in mammalian accessory olfactory bulb. Microsc Res Tech *43*, 476-499.

Meredith, M. (2001). Human vomeronasal organ function: a critical review of best and worst cases. Chem Senses *26*, 433-445.

Miyamichi, K., Amat, F., Moussavi, F., Wang, C., Wickersham, I., Wall, N.R., Taniguchi, H., Tasic, B., Huang, Z.J., He, Z.*, et al.* (2011). Cortical representations of olfactory input by trans-synaptic tracing. Nature *472*, 191-196.

Mombaerts, P., Wang, F., Dulac, C., Chao, S.K., Nemes, A., Mendelsohn, M., Edmondson, J., and Axel, R. (1996). Visualizing an olfactory sensory map. Cell *87*, 675-686.

Mori, K., and Sakano, H. (2011). How is the olfactory map formed and interpreted in the mammalian brain? Annu Rev Neurosci *34*, 467-499.

Nagai, Y., Sano, H., and Yokoi, M. (2005). Transgenic expression of Cre recombinase in mitral/tufted cells of the olfactory bulb. Genesis *43*, 12-16.

Niimura, Y. (2009). On the origin and evolution of vertebrate olfactory receptor genes: comparative genome analysis among 23 chordate species. Genome Biol Evol *1*, 34-44.

Nyby, J., Wysocki, C.J., Whitney, G., and Dizinno, G. (1977). Pheromonal regulation of male mouse ultrasonic courtship (Mus musculus). Anim Behav *25*, 333-341.

Oka, Y., Katada, S., Omura, M., Suwa, M., Yoshihara, Y., and Touhara, K. (2006). Odorant receptor map in the mouse olfactory bulb: in vivo sensitivity and specificity of receptor-defined glomeruli. Neuron *52*, 857-869.

Ressler, K.J., Sullivan, S.L., and Buck, L.B. (1994). Information coding in the olfactory system: evidence for a stereotyped and highly organized epitope map in the olfactory bulb. Cell *79*, 1245-1255.

Root, C.M., Denny, C.A., Hen, R., and Axel, R. (2014). The participation of cortical amygdala in innate, odour-driven behaviour. Nature *515*, 269-273.

Scalia, F., and Winans, S.S. (1975). The differential projections of the olfactory bulb and accessory olfactory bulb in mammals. J Comp Neurol *161*, 31-55.

Schaefer, M.L., Young, D.A., and Restrepo, D. (2001). Olfactory fingerprints for major histocompatibility complex-determined body odors. J Neurosci *21*, 2481-2487.

Schambra, U.B., Lauder, J.M., and Silver, J. Atlas of the mouse brain (Academic press).

Schwob, J.E., and Price, J.L. (1984). The development of axonal connections in the central olfactory system of rats. J Comp Neurol *223*, 177-202.

Serizawa, S., Miyamichi, K., Takeuchi, H., Yamagishi, Y., Suzuki, M., and Sakano, H. (2006). A neuronal identity code for the odorant receptor-specific and activity-dependent axon sorting. Cell *127*, 1057-1069.

Shipley, M.T., and Adamek, G.D. (1984). The connections of the mouse olfactory bulb: a study using orthograde and retrograde transport of wheat germ agglutinin conjugated to horseradish peroxidase. Brain Res Bull *12*, 669-688.

Sosulski, D.L., Bloom, M.L., Cutforth, T., Axel, R., and Datta, S.R. (2011). Distinct representations of olfactory information in different cortical centres. Nature *472*, 213-216.

Stowers, L., Holy, T.E., Meister, M., Dulac, C., and Koentges, G. (2002). Loss of sex discrimination and male-male aggression in mice deficient for TRP2. Science *295*, 1493-1500.

Stowers, L., and Marton, T.F. (2005). What is a pheromone? Mammalian pheromones reconsidered. Neuron *46*, 699-702.

Suarez, R., Garcia-Gonzalez, D., and de Castro, F. (2012). Mutual influences between the main olfactory and vomeronasal systems in development and evolution. Front Neuroanat *6*, 50.

Takeuchi, H., Inokuchi, K., Aoki, M., Suto, F., Tsuboi, A., Matsuda, I., Suzuki, M., Aiba, A., Serizawa, S., Yoshihara, Y.*, et al.* (2010). Sequential arrival and graded secretion of Sema3F by olfactory neuron axons specify map topography at the bulb. Cell *141*, 1056-1067.

Treloar, H.B., Gabeau, D., Yoshihara, Y., Mori, K., and Greer, C.A. (2003). Inverse expression of olfactory cell adhesion molecule in a subset of olfactory axons and a subset of mitral/tufted cells in the developing rat main olfactory bulb. J Comp Neurol *458*, 389-403.

Tsuboi, A., Yoshihara, S., Yamazaki, N., Kasai, H., Asai-Tsuboi, H., Komatsu, M., Serizawa, S., Ishii, T., Matsuda, Y., Nagawa, F*., et al.* (1999). Olfactory neurons expressing closely linked and homologous odorant receptor genes tend to project their axons to neighboring glomeruli on the olfactory bulb. J Neurosci *19*, 8409-8418.

Tummala, R., Romano, R.A., Fuchs, E., and Sinha, S. (2003). Molecular cloning and characterization of AP-2 epsilon, a fifth member of the AP-2 family. Gene *321*, 93-102.

Vassar, R., Chao, S.K., Sitcheran, R., Nunez, J.M., Vosshall, L.B., and Axel, R. (1994). Topographic organization of sensory projections to the olfactory bulb. Cell *79*, 981-991.

Walz, A., Omura, M., and Mombaerts, P. (2006). Development and topography of the lateral olfactory tract in the mouse: imaging by genetically encoded and injected fluorescent markers. J Neurobiol *66*, 835-846.

Walz, A., Rodriguez, I., and Mombaerts, P. (2002). Aberrant sensory innervation of the olfactory bulb in neuropilin-2 mutant mice. J Neurosci *22*, 4025-4035.

Wickersham, I.R., Lyon, D.C., Barnard, R.J., Mori, T., Finke, S., Conzelmann, K.K., Young, J.A., and Callaway, E.M. (2007). Monosynaptic restriction of transsynaptic tracing from single, genetically targeted neurons. Neuron *53*, 639-647.

Yan, Z., Tan, J., Qin, C., Lu, Y., Ding, C., and Luo, M. (2008). Precise circuitry links bilaterally symmetric olfactory maps. Neuron *58*, 613-624.

Yoshihara, Y., Mizuno, T., Nakahira, M., Kawasaki, M., Watanabe, Y., Kagamiyama, H., Jishage, K., Ueda, O., Suzuki, H., Tabuchi, K*., et al.* (1999). A genetic approach to visualization of multisynaptic neural pathways using plant lectin transgene. Neuron *22*, 33-41.

Yoshikawa, K., Nakagawa, H., Mori, N., Watanabe, H., and Touhara, K. (2013). An unsaturated aliphatic alcohol as a natural ligand for a mouse odorant receptor. Nat Chem Biol *9*, 160-162.

7. Acknowledgments

I would like to thank Dr. Yoshihiro Yoshihara for Goofy-Cre mouse, Dr. Trevor Williams for AP2ε-Cre mouse, Dr. Edward M Callaway for RV and TVA vectors, Dr. Eric Block and Dr. Hiroaki Matsunami for MTMT. I would like to thank Dr. Fumiaki Imamura for *in utero* electroporation study.

I am grateful to lab members for valuable comments and discussion. I would like to thank Dr. Haruki Takeuchi for teaching and valuable discussion. I am grateful to Prof. Hitoshi Sakano for the continuous support of my research.